NASA TECHNICAL REPORT

NASA TR R-387

NASA TR R-387
c. 1

MAXIMUM RANGE THREE-DIMENSIONAL LIFTING PLANETARY ENTRY

by E. D. Dickmanns

George C. Marshall Space Flight Center
Marshall Space Flight Center, Ala. 35812

NATIONAL AERONAUTICS AND SPACE ADMINISTRATION • WASHINGTON, D. C. • AUGUST 1972

1. Report No.	2. Government Accession No.	3. Recipient's Catalog No.
NASA TR R-387		

4. Title and Subtitle	5. Report Date
Maximum Range Three-Dimensional Lifting Planetary Entry	August 1972
	6. Performing Organization Code

7. Author(s)	8. Performing Organization Report No.
E. D. Dickmanns	10. Work Unit No.

9. Performing Organization Name and Address	11. Contract or Grant No.
George C. Marshall Space Flight Center Marshall Space Flight Center, Alabama 35812	13. Type of Report and Period Covered
	Technical Report

12. Sponsoring Agency Name and Address	14. Sponsoring Agency Code
National Aeronautics and Space Administration Washington, D. C. 20546	

15. Supplementary Notes

Prepared by Aero-Astrodynamics Laboratory, Science and Engineering.
This research was sponsored by a Postdoctoral Research Associateship through the National Academy of Sciences.

16. Abstract

Variational equations for maximum range three-dimensional quasisteady glide are given. Nonlinear oscillatory maximum range trajectories obtained with a refined gradient program are approximated by a superposition of quasisteady glide and linearized perturbation equation results. A "basic" control law is found which is closely followed for maximum cross-range trajectories.

The effect of a reradiative heating constraint involving velocity, altitude and angle of attack on a maximum cross-range trajectory for a Space Shuttle orbiter-type vehicle reentering the earth's atmosphere is investigated numerically.

17. Key Words (Suggested by Author(s))	18. Distribution Statement
Entry Trajectories Optimization Constraint Space Shuttle Crossrange	

19. Security Classif. (of this report)	20. Security Classif. (of this page)	21. No. of Pages	22. Price*
Unclassified	Unclassified	52	$3.00

* For sale by the National Technical Information Service, Springfield, Virginia 22151

TABLE OF CONTENTS

LIST OF ILLUSTRATIONS

LIST OF ILLUSTRATIONS (Concluded)

LIST OF SYMBOLS

Symbol	Definition
$A_{i,j}$	time-varying coefficient matrix for state perturbation, equations (4.2.3), (4.2.5)
a	$\rho_0 Sr/(2m)$ wingloading-atmospheric density parameter
$B_{i,j}$	time-varying coefficient matrix for control perturbations, equations (4.2.3), (4.2.6)
B_i	auxiliary array for computing heating constraint (section 3.4)
b	scaling factor in heating constraint representation (section 3.4)
b	$\sqrt{v}\ a \exp(-\beta h)$ abbreviation in $B_{i,j}$ matrix
C	(inequality) constraint equation
C_i	auxiliary array for computing heating constraint (section 3.4)
C_D	drag coefficient $\left(C_{D0} + k C_L^{\,n}\right)$
C_{D0}	zero lift drag coefficient
C_L	lift coefficient
C_{LE}	lift coefficient for maximum L/D $\left[\left(L/D\right)_{max} = E\right]$
C_{LH}	lift coefficient determined from heating constraint
ΔC_{LH}	parameter to shift heating constraint
D	drag force
d	dimensional quantity

LIST OF SYMBOLS (Continued)

Symbol	Definition
E	maximum lift-to-drag ratio L/D
e	total mechanical energy per unit mass (v/2 + h)
f	vector of right-hand side of differential equations
$G_{i,j}$	matrix of generating coefficients for heating constraint (section 3.4)
g	gravitational acceleration
H	variational Hamiltonian
H_i	auxiliary array for computing heating constraint (section 3.4)
h	altitude (nondimensionalized by radius vector |r|)
h_{ek}	kinetic energy altitude
k	factor for lift-dependent drag term
L	lift force
l	total range variable
Ma	Mach number
m	vehicle mass
n	power of lift-dependent drag term
p	factor to form three-dimensional range payoff quantity
QSG	quasisteady glide; this term is preferred over "equilibrium glide" since in the three-dimensional case, only one out of three force components is in equilibrium

LIST OF SYMBOLS (Continued)

Symbol	Definition
R	planet radius
r	distance from vehicle center of gravity to planet center
S	aerodynamic reference area
s	independent variable in Laplace transform
t	time (nondimensionalized by $\sqrt{r/g}$)
u	controls
V	dimensional velocity
v	nondimensionalized velocity $v = V^2/rg$
w	equation (4.1.32) auxiliary variable to determine optimal controls
x, y, z	Cartesian coordinates (indexed)
x	vector of state variables

Greek Symbols	Definition
α	angle of attack
β	inverse atmospheric scale height 1/6.9 [km^{-1}] for earth nondimensionalized by r, $\beta \approx 930$ for earth
γ	flight path angle
$\delta( )$	perturbation quantity
ϕ	heating constraint surface
Λ	lateral range angle

LIST OF SYMBOLS (Continued)

Greek Symbols	Definition
λ	Lagrangian multipliers (indexed by corresponding state variable)
λ_1	instable real root of perturbation characteristic equation
μ	aerodynamic bank angle ($\measuredangle$ lift force and vertical plane)
ν	multiplier to algebraic vertical equilibrium equation
χ	heading angle
ρ	atmospheric density
Θ	downrange angle
τ	nondimensional time (for earth: $\sqrt{r/g} \approx 815$ sec)
ζ	damping ratio of oscillatory perturbation component

Indices	Definition
c	constrained
E	for maximum L/D
f	at final time
i, j	running indices
opt	satisfying the necessary conditions for optimality
Q or QSG	quantity from quasisteady glide solution
S	local circular satellite quantity
uc	unconstrained
0	initial condition or quantity at sea level

LIST OF SYMBOLS (Concluded)

Other Symbols

$\dot{(\ )} = \frac{d}{dt}(\ )$ time derivative

$\overset{\circ}{(\ )} = \frac{d}{d\tau}(\ )$ nondimensional time derivative

MAXIMUM RANGE THREE-DIMENSIONAL LIFTING PLANETARY ENTRY

I. INTRODUCTION

With the advent of the Space Shuttle, lifting reentry trajectories with medium lift-to-drag ratio (L/D) become of practical interest. Trajectories for this type of vehicle have, however, been investigated for a long time. The downrange capabilities were first discussed by Sänger [1] in 1933 and later on were studied by many investigators (see, e.g., References 2 and 3). The trajectories are, in general, oscillatory and can be thought of as a quasisteady-glide (QSG) component (with $\dot{\gamma} = 0$) superimposed by a perturbation (with time-varying frequency and damping in the linear approximation). The QSG solution is an algebraic relationship between density, velocity, and lift coefficient, and this problem is readily solved for constant L/D. For small deviations from QSG, the equations may be linearized (Campbell [4]) or approximated by higher order expansions (Hanin [5]) to obtain frequency and damping of the actual trajectory. Recently Shi, et al. [6 and 7] using matched asymptotic expansions were able to achieve analytical approximate solutions to the nonlinear equations for a wide range of entry parameters.

Cross-range investigations have appeared in the literature since about 1960 [8 through 13]. Because of the increased dimension and nonlinearity of this problem, analytical solutions are even more sparse than for planar entry, and most investigations involve numerical computations. Eggers [8], Slye [9], and Jackson [10] consider a constant bank angle QSG maneuver. London [12] commented on the influence of the centrifugal term in the heading differential equation for these solutions. The equations obtained by Jackson for a spherical earth lend themselves to consider a bank angle program as a function of velocity and lateral range [11]. This minor circle turn is further discussed in References 13 through 16.

In this report, a variational formulation for footprint maximization under QSG conditions is given. For a special case, some analytical approximate integrals are obtained. For an entry vehicle with L/D = 1.4, QSG-footprint trajectories resulting from a numerical initial value search/trajectory optimization procedure are given. The perturbation equations around three-dimensional QSG trajectories are derived and discussed together with numerical solutions of non-QSG trajectories. Finally, the influence of a heating constraint on a maximum lateral range non-QSG reentry trajectory is discussed for a Space Shuttle orbiter-type vehicle.

2. COORDINATE SYSTEM

The equations of motion are written in a flight path oriented axis system, the x-axis of which is aligned with the velocity vector. The z-axis is downward in the vertical plane, and the origin of this right-handed system is based in the vehicle center of gravity (c.g.). The position of the vehicle c.g. with respect to the planet is specified by the downrange angle Θ, the cross-range angle Λ and the radial distance $r = R + h$ (Fig. 1). The heading angle relative to the initial conditions is designated by χ, positive for right turns.

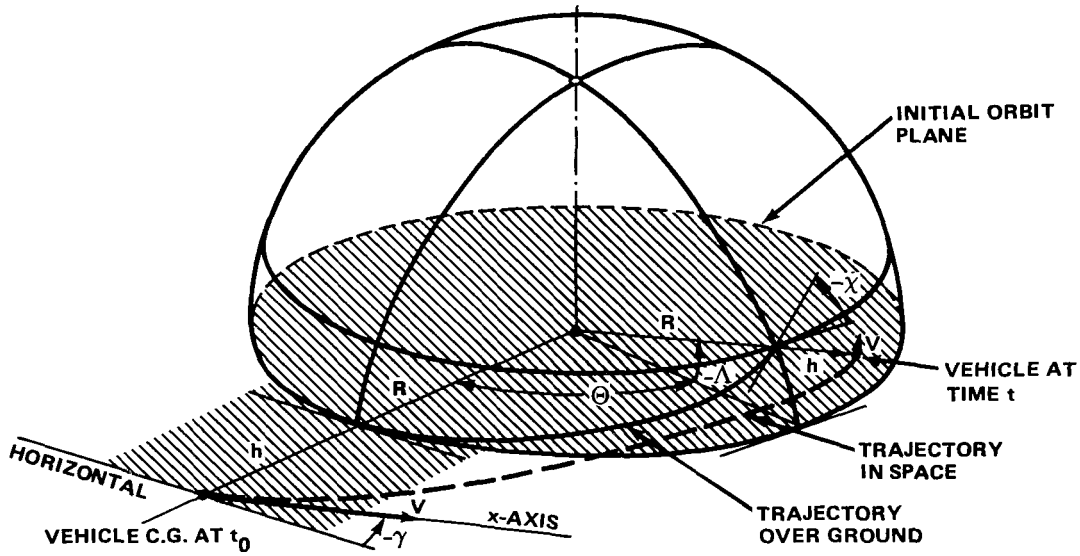

Figure 1. Coordinate system.

3. MATHEMATICAL MODEL AND SIMPLIFYING ASSUMPTIONS

3.1 Planet Model

Because of the planet rotation, the oblateness, and the variation of the atmospheric properties with location and time, an actual entry trajectory depends on location, direction, and time of entry. For general entry trajectory investigations, a reduction of the possible parameter combinations is

often desirable. The dependency of the trajectory on entry time is eliminated by assuming

(A1) a stationary atmosphere,

the dependency on entry point and direction by the following three assumptions:

(A2) no planet rotation,

(A3) no wind,

(A4) planet and atmosphere are point symmetric (homogeneous on sphere-shells).

Assumption (A4) eliminates the oblateness effects and the latitudinal variations of the atmosphere. For earth reentry with satellite velocity along the equator, assumption (A2) leads to errors of approximately

6 percent in the aerodynamic velocity,

12 percent in dynamic pressure,

20 percent in the heating rate,

initially. For meridional entry, the errors are much smaller. Best approximations to actual trajectories can be expected with these assumptions for meridional entries in high latitudes. These assumptions about the planet considerably reduce the variational equations for reentry.

Since the purpose of this report is to investigate basic properties of maximum range trajectories, they will be adopted along with others simplifying the vehicle model. The influence of oblateness and earth rotation on reentry trajectories is discussed in References 17, 18, and 19. The last two references also touch on the effect of assuming

(A5) an exponential density law, $\rho = \rho_0 \exp(-\beta h)$,

which is convenient for analytical computations.

3.2 Vehicle Model

The vehicle is assumed to be

(A6) a point mass with instantaneous angular control.

The aerodynamic characteristics are assumed to be

(A7) independent of Mach number and altitude

and to obey the relationship (drag polar)

(A8) $C_D = C_{D0} + k C_L^n$.

Assumption (A8) is a good representation for maximum range trajectories, which are flown in the vicinity of $(L/D)_{max}$. The consequence of assumption (A7) is to eliminate viscous interaction effects for high altitudes, which may have an appreciable influence on maximum range trajectories as shown in Reference 20. This can be accounted for partly by using a "medium" drag polar. Mach number effects become dominant in the supersonic and subsonic region which are not considered here. The trajectories are ended in 30 km altitude corresponding to about Ma = 3 . Although in the latter part of the trajectory, the dependency on the Mach number shows up, assumption (A7) is adopted throughout to reduce the number of parameters involved.

3.3 Assumptions for Analytical Solution

Further assumptions to obtain analytical approximate solutions are

(A9) small flight path angles: $\cos\gamma = 1$, $\sin\gamma = \gamma$

(A10) potential energy << kinetic energy: $e \approx v/2$

(A11) cylindrical planet: $\cos\Lambda = 1$
horizontal centrifugal component << aerodynamic turn force

(A12) Quasisteady-glide: $\dot{\gamma} = 0$.
The flight path angle will be determined from a differentiation of the QSG solution.

3.4 Radiative Heating Constraint

The heating constraint for a reentry vehicle is one of the driving factors in trajectory shaping. Medium- (like the proposed Space Shuttle orbiter) and high-L/D vehicles have a thermal protection system (TPS) consisting of reradiative and ablative elements at different parts of the vehicle

[21]. The higher the L/D, the more reradiative the TPS is going to be. If the time constants for the outer skin to heat up to the design limit is small compared to the rate at which the vehicle state (especially altitude, angle of attack, and velocity) changes, then a quasisteady approximation is valid. In this case, the heating constraint can be formulated as an algebraic equation $\phi(V,h,\alpha) = 0$, where V is the aerodynamic velocity, h is the altitude (representing air density), and α is the angle of attack of the vehicle. It is assumed that the sideslip angle β is kept small so that its influence can be neglected.

The data underlying the present representation are taken from Reference 22 for a limit temperature of 2000° F. Figure 2a shows a qualitative picture of typical altitude constraints due to dynamic pressure and kinetic heating. The effects of both velocity and lift coefficient are seen to be appreciable for the heating constraint. The heating constraint is more severe than the dynamic pressure boundary for hypersonic speeds ($V > 2.5$ to 4.5 km/s depending on the angle of attack). In the trajectory optimization program, on a boundary arc, the control C_{LH} is required as a function of the state variables altitude and velocity. The data are given in the form [22]

$$\phi(h,V,\alpha) = 0 \quad . \tag{3.1}$$

Since the use of the lift coefficient C_L instead of angle of attack α reduces the computational workload to represent the aerodynamic characteristics of the vehicle, the relation $C_L(\alpha,h,V)$ is used to eliminate α. The transformed equation (3.1) is, then, represented in the form

$$C_{LH} = B_i H_i + \Delta C_{LH} \quad , \; i = 1,5 \tag{3.2}$$

where

$$\left.\begin{aligned} B_i &= g_{i,j}\, \hat{h}^{(j-1)} \quad , \; j = 1,4 \quad ; \\ H_1 &= bh^2/V^2 \\ H_2 &= bh/V - H_1 \\ H_3 &= 1 - bh/V - H_2 \\ H_4 &= V/(bh) - 2 + bh/V - H_3 \\ H_5 &= V^2/(bh)^2 - 3V/(bh) + 3 - bh/V - H_4 \end{aligned}\right\} \quad ; \tag{3.3}$$

and ΔC_{LH} is an adjustment parameter; $g_{i,j}$ is a coefficient matrix

$$\begin{bmatrix} 0.110717 & 0.834519 & 1.213679 & -1.060833 \\ -0.672677 & 2.734170 & -0.864369 & -12.100000 \\ 0.812241 & 2.337815 & 10.316280 & 22.974860 \\ -3.151267 & -13.621310 & -40.485500 & -57.833330 \\ 2.368095 & 19.073400 & 69.869050 & 127.777778 \end{bmatrix} \quad ; \quad (3.4)$$

$\hat{h}$ is a coordinate transformed altitude

$$\hat{h} = h/50[\text{km}] - 1 \qquad (3.5)$$

to keep the coefficients closer to 1 . The constant $b = 0.095$ serves the same purpose for the velocity. This form has been arrived at by intuition and trial. It is a bivariate polynomial of third order in the altitude and fourth order in velocity. With

$$C_i = \sum_{j=1}^{4} (j-1)\, g_{i,j}\, \hat{h}^{(j-2)} \quad , \qquad (3.6)$$

the partial derivatives may be written

$$\partial C_{LH}/\partial V = B_i\, \partial/\partial V(H_i) \qquad (3.7)$$

$$\partial C_{LH}/\partial h = C_i\, H_i + B_i\, \partial/\partial h(H_i) \quad . \qquad (3.8)$$

From the form (3.1) one obtains for constant C_{LH} the partial

$$\left.\frac{\partial h}{\partial V}\right|_{C_{LH}} = -\frac{\dfrac{\partial C_{LH}}{\partial V}}{\dfrac{\partial C_{LH}}{\partial H}} \quad . \qquad (3.9)$$

The function generated in this way is shown in Figure 2b.

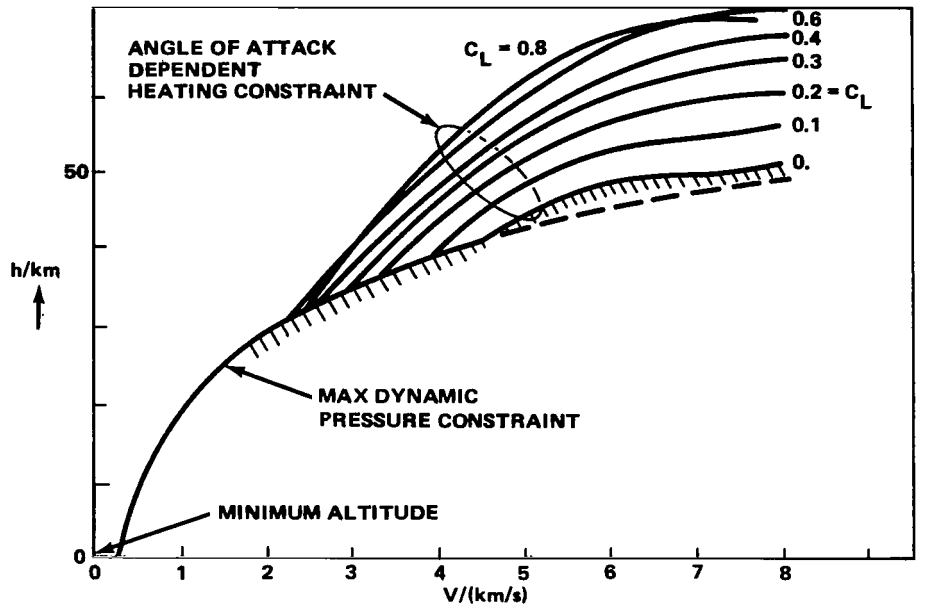

a. Qualitative altitude constraints for reentry.

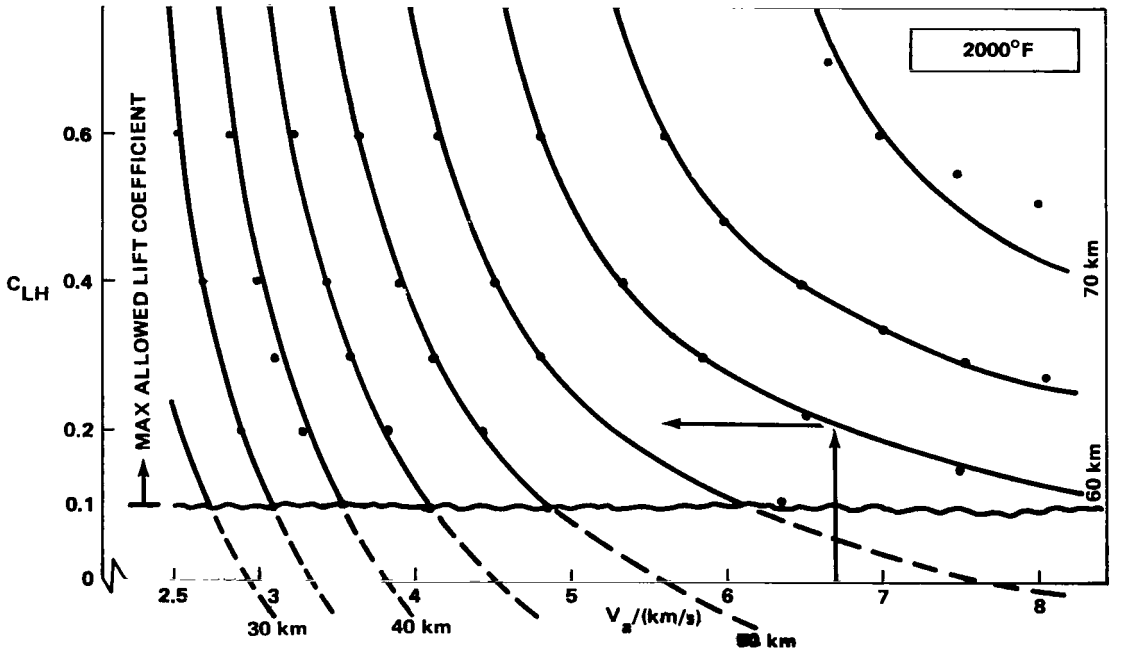

b. Bivariate heating constraint approximation.

Figure 2. Reradiative heating constraint for Space Shuttle orbiter-type reentry vehicle.

The accuracy of the approximation is indicated in Figure 2b by dots representing the original input data into the curve fit procedure. These points had been obtained from Reference 22 through a crossplot. Except for the 70-km curve, the approximation is good considering the uncertainty in the original data. For maximum range and minimum energy loss trajectories which result in lift coefficients in the vicinity of maximum L/D (around $C_L = 0.2$), the 70-km curve will not be needed. Aside from that, the deviation is on the safe side.

4. EQUATIONS OF MOTION

Under the assumptions made, the equations of motion may be written:

$$\dot{V} = - g \sin\gamma - \frac{D}{m} \tag{4.1.1}$$

$$\dot{\chi} = - \frac{V}{r} \cos\gamma \cos\chi \tan\Lambda + \frac{L}{mV} \frac{\sin\mu}{\cos\gamma} \tag{4.1.2}$$

$$\dot{\gamma} = \left(\frac{V}{r} - \frac{g}{V}\right) \cos\gamma + \frac{L}{mV} \cos\mu \tag{4.1.3}$$

$$\dot{\Theta} = \frac{V}{r} \frac{\cos\gamma}{\cos\Lambda} \cos\chi \tag{4.1.4}$$

$$\dot{\Lambda} = \frac{V}{r} \cos\gamma \sin\chi \tag{4.1.5}$$

$$\dot{r} = \dot{h}_d = V \sin\gamma \tag{4.1.6}$$

where

$$\begin{bmatrix} L \\ D \end{bmatrix} = \begin{bmatrix} C_L \\ C_D \end{bmatrix} S \frac{\rho}{2} V^2 \qquad \begin{matrix} \text{lift} \\ \text{drag} \end{matrix} \quad , \tag{4.1.7}$$

exponential atmosphere

$$\rho = \rho_0 \exp\left(-\beta_d h_d\right) \quad , \tag{4.1.8}$$

gravity acceleration

$$g = g_0 R^2/\left(R + h_d\right)^2 \quad . \tag{4.1.9}$$

The lift coefficient C_L and the bank angle μ are controls. For analytical solutions, a nondimensionalized form of these equations is advantageous. With the nondimensional time,

$$\tau = t\sqrt{g/r} \tag{4.1.10}$$

and

$$v = V^2/(rg) \quad , \quad h = h_d/r \tag{4.1.11}$$

these equations (4.1.1) to (4.1.7) become the following, where

$$\left(\,\dot{}\,\right) = \frac{d}{d\tau}\left(\,\right) \quad , \quad a = \frac{\rho_0 S r}{2m} \quad , \tag{4.1.12}$$

$$\dot{v} = -\sqrt{v}\,2\left[a \exp(-\beta h)\, C_D\, v + \sin\gamma\right] \tag{4.1.13}$$

$$\dot{\chi} = \sqrt{v}\left[a \exp(-\beta h)\, C_L \sin\mu/\cos\gamma - \cos\gamma \cos\chi \tan\Lambda\right] \tag{4.1.14}$$

$$\dot{\gamma} = \sqrt{v}\left[a \exp(-\beta h)\, C_L \cos\mu - (1 - v)/v \cos\gamma\right] \tag{4.1.15}$$

$$\dot{\Theta} = \sqrt{v} \cos\gamma \cos\chi/\cos\Lambda \tag{4.1.16}$$

$$\dot{\Lambda} = \sqrt{v} \cos\gamma \sin\chi \tag{4.1.17}$$

$$\dot{h} = \sqrt{v} \sin\gamma \quad . \tag{4.1.18}$$

The reciprocal atmospheric scale height now has approximately the value (for earth)

$$\beta \approx 930 \quad . \tag{4.1.19}$$

The solution to these equations for maximum range trajectories will now be approximated by superposition of two motion components:

1. A QSG motion with equation (4.1.15) satisfied by $\dot{\gamma} = 0$

2. A small perturbation around the QSG trajectory.

4.1 Quasisteady-glide Maximum Range

4.1.1 VARIATIONAL QSG-EQUATIONS

By introducing the specific energy

$$e = v/2 + h \tag{4.1.20}$$

and adding equations (4.1.13) and (4.1.18), the nondimensional altitude h becomes control-like, and, with $v = 2(e - h)$ from equation (4.1.20) and applying assumption (A2), the following set of equations are obtained for the analytical QSG solution:

$$\mathring{e} = -\sqrt{2(e - h)}\, a \exp(-\beta h)\, C_D\, 2(e - h) \tag{4.1.21}$$

$$\mathring{\chi} = \sqrt{2(e - h)}\, \left[a \exp(-\beta h)\, C_L \sin\mu/\cos\gamma - \cos\gamma \cos\chi \tan\Lambda \right] \tag{4.1.22}$$

$$\mathring{\Theta} = \sqrt{2(e - h)}\, \cos\gamma \cos\chi/\cos\Lambda \tag{4.1.23}$$

$$\mathring{\Lambda} = \sqrt{2(e - h)}\, \cos\gamma \sin\chi \tag{4.1.24}$$

$$\sqrt{2(e - h)} \left(a \exp(-\beta h)\, C_L \cos\mu - \left\{ 1/[2(e - h)] - 1 \right\} \cos\gamma \right) = 0 \,. \tag{4.1.25}$$

These are four differential equations and one algebraic one, equation (4.1.25), which, however, has to be satisfied all along the trajectory.

All initial conditions of the differential equations are considered to be given, while the initial altitude has to be found such that the payoff quantity obtains its extremum. This is an optimization problem with mixed side constraints [23]. The variational Hamiltonian is

$$H = \sqrt{2(e-h)}\left\{a \exp(-\beta h)\left[-\lambda_e C_D 2(e-h) + C_L\left(\frac{\lambda_\chi}{\cos\gamma}\sin\mu + \nu\cos\mu\right)\right]\right.$$
$$\left. + \left[\left(-\lambda_\chi \tan\Lambda + \lambda_\Theta/\cos\Lambda\right)\cos\chi + \lambda_\Lambda \sin\chi - \nu\left(\frac{1}{2(e-h)} - 1\right)\right]\cos\gamma\right\} \tag{4.1.26}$$

and, since final time is open, the bracket $\{\ \}$ is zero. ν is a time-varying multiplier associated with the equality constraint (4.1.25) and will be determined as a linear combination of the multipliers λ [23].

For a moment, eliminate equation (4.1.25) by introducing it into equations (4.1.21) and (4.1.22) in order to obtain a convenient expression for the optimal lift coefficient. Later on, however, one continues with the mixed side constraint formulation. One obtains

$$\dot{e} = -\sqrt{v}\,\frac{1-v}{E\cos\mu}\cos\gamma \quad , \tag{4.1.27}$$

where

$$E = C_L/C_D$$

$$\dot{\chi} = \sqrt{v}\left(\frac{\tan\mu}{\cos\gamma} - \cos\gamma\cos\chi\tan\Lambda\right) \quad , \tag{4.1.28}$$

and the control-dependent part of the Hamiltonian in this formulation is with $\cos\gamma \approx 1$:

$$H^* = \sqrt{v}\left\{-\lambda_e\,\frac{(1-v)}{E\cos\mu} + \lambda_\chi\tan\mu + \ldots\right\} \tag{4.1.29}$$

$\partial H^*/\partial C_L = 0$ yields $\partial E/\partial C_L = 0$, i.e., the lift-to-drag ratio (4.1.30)

E has to be a maximum for a maximum range QSG trajectory. Since the aerodynamic drag polar is considered to be constant in the hypersonic range considered, E is a constant as well as C_{LE}, the corresponding lift coefficient. This information will be used when one returns, now, to the mixed formulation (4.1.26).

Looking for the extremum of the Hamiltonian with respect to the controls C_L, μ and altitude h yields for maximum range $\left(\min_u H \right)$:

Bank angle:

$$\tan \mu_{opt} = \frac{\lambda_\chi}{\nu \cos \gamma} \tag{4.1.31}$$

or

$$\sin \mu = \lambda_\chi / (- w \cos \gamma) \quad , \quad \cos \mu = \nu / (-w) \quad ,$$

$$w = \left(\nu^2 + \lambda_\chi^2 / \cos^2 \gamma \right)^{1/2} \quad . \tag{4.1.32}$$

Optimal lift coefficient:

$$\left. \frac{\partial C_D}{\partial C_L} \right|_{C_{LE}} = \frac{-w}{\lambda_e v} = \frac{1}{E} \quad . \tag{4.1.33}$$

From equation (4.1.30) one concludes that $w/(v\lambda_e)$ is a constant. Its value is the inverse of the lift-to-drag ratio. $\partial H/\partial h = 0$ furnishes the relationship

$$a \exp(-\beta h) \left[\lambda_e C_{DE} (\beta v + 2) + \beta w C_{LE} \right] - \frac{2\nu}{v^2} \cos \gamma = 0 \quad , \tag{4.1.34}$$

or

$$\left[a \exp(-\beta h) C_D \right]_{opt} = \frac{2\nu}{v^2 \left[\lambda_e (\beta v + 2) + \beta E w \right]} \quad ,$$

which with equation (4.1.33) reduces to

$$\left[a \exp(-\beta h) C_D \right]_{opt} = \frac{\nu}{\lambda_e v^2} \quad . \tag{4.1.35}$$

Combining this with the QSG equation (4.1.25) yields

$$\nu = \frac{\lambda_e}{E}\, v\sqrt{(1 - v)} \quad . \tag{4.1.36}$$

From equation (4.1.26), the differential equations for the Lagrangian multipliers become (final time open, $H \equiv 0$)

$$\dot{\lambda}_e = -\sqrt{2(e - h)}\left[a \exp(-\beta h)\, C_D\, 2\left(-\lambda_e\right) + \nu \frac{1}{2(e - h)^2}\right]$$

and with equation (4.1.35)

$$\dot{\lambda}_e = 0 \quad \text{or} \quad \lambda_e = \text{const.} \tag{4.1.37}$$

$$\dot{\lambda}_\chi = -\sqrt{2(e - h)}\left[\left(\lambda_\Theta - \lambda_\chi \sin\Lambda\right)(-\sin\chi) + \lambda_\Lambda \cos\chi\right] \tag{4.1.38}$$

$$\dot{\lambda}_\Theta = 0 \quad \text{or} \quad \lambda_\Theta = \text{const.} \tag{4.1.39}$$

$$\dot{\lambda}_\Lambda = \sqrt{2(e - h)}\, \frac{\cos\chi}{\cos^2\Lambda}\left(\lambda_\chi - \lambda_\Theta \sin\Lambda\right) \quad . \tag{4.1.40}$$

There are only two differential equations for the adjoints, and because of $\lambda_e = \text{const.}$ the multiplier ν is a function of v alone.

The boundary conditions for maximum-range-QSG with a given kinetic energy decrease $\frac{1}{2}\left(v_0 - v_f\right)$ and open final heading angle are

at t_0	at t_f	multiplier at t_f
v_0 = given	v_f = given	λ_{e_f} = unknown = λ_e
$\chi_0 = 0$	χ_f = open	$\lambda_{\chi_f} = 0$
$\Theta_0 = 0$	$\phi = \Lambda + p\Theta = \max$	$\lambda_\Theta = -p$
$\Lambda_0 = 0$	$H(t_f) = 0$	(see section 4.3.3)
		$\lambda_{\Lambda_f} = -1$

h_0 , μ_0 , γ_0 have to be found such as to maximize the payoff quantity ϕ .

From $\lambda_{\chi_f} = 0$ and equation (4.1.31) the equation for the final bank angle follows:

$$\mu_f = 0 \quad . \tag{4.1.41}$$

Differentiating the QSG equation (4.1.25) with respect to time and inserting equations (4.1.13) and (4.1.18), an expression for the flight path angle is obtained:

$$\sin\gamma = -\frac{1-v}{\cos\mu}\,\frac{2/E+\sqrt{v}\,\overset{\circ}{\mu}\sin\mu}{2+(1-v)\beta v} \quad . \tag{4.1.42}$$

With equation (4.1.41) for the final time, this reduces to

$$E\sin\gamma_f = \frac{-2(1-v)}{2+(1-v)\beta v} \quad . \tag{4.1.42a}$$

Compared with results from numerical optimizations, this equation predicts the final flight path angle with good accuracy. It is the same as for planar entry. Except for the final time, the flight path angle is a function of the bank angle and its rate of change, however.

4.1.2 SOME ANALYTICAL APPROXIMATE RESULTS FOR MAXIMUM CROSS-RANGE

With $\lambda_\Theta = 0$, which characterizes this case, and assumptions (A9) to (A11), the variational QSG equations reduce to

$$\left.\begin{aligned}
\overset{\circ}{v} &= -2\sqrt{v}\left[\frac{a}{l}\exp(-\beta h)\,C_D\,v\right] & \overset{\circ}{\lambda}_e &= 0\\
\overset{\circ}{\chi} &= \sqrt{v}\,a\exp(-\beta h)\,C_L\sin\mu & \overset{\circ}{\lambda}_\chi &= -\sqrt{v}\,\lambda_\Lambda\cos\chi\\
\overset{\circ}{\Theta} &= \sqrt{v}\cos\chi & \overset{\circ}{\lambda}_\Theta &= 0\\
\overset{\circ}{\Lambda} &= \sqrt{v}\sin\chi & \overset{\circ}{\lambda}_\Lambda &= \sqrt{v}\,\lambda_\chi\cos\chi
\end{aligned}\right\} \tag{4.1.43}$$

$$a \exp(-\beta h)\, C_{LE} \cos\mu = (1 - v)/v \qquad \text{(QSG)}$$

$$\tan\mu_{opt} = \lambda_\chi/\nu \qquad \text{with } \nu = \lambda_e v\sqrt{1 - v}/E$$

$$C_{L\,opt} = C_{LE} \qquad \text{where } E = (L/D)_{max} = -v\lambda_e/\left(\lambda_\chi^2 + \nu^2\right)^{1/2}$$

Combining the last two lines with three equations for the four quantities μ, λ_χ, ν, and the product $(\lambda_e v)$ yields the surprising result

$$\tan\mu = \sqrt{v/(1 - v)} \quad \text{or} \quad \sin\mu = \sqrt{v} \quad . \tag{4.1.44}$$

Note that this simple relationship for the bank angle as a function of the velocity (μ = arc sin of the ratio velocity to local satellite velocity) has been obtained from the three relations $\partial H/\partial u = 0$, $u^T = (C_L, \mu, h)$, together with the QSG condition without taking into account any boundary conditions. Therefore, this solution will be called "basic" and will be regarded with due suspicion. It may further be noted that this bank angle program has a square root relationship to the minor circle turn bank angle program [11, 13 through 16]. This solution is discussed below.

4.1.2.1 "Basic" Solution. Differentiation of equation (4.1.44) with respect to time yields, with equations (4.1.13) and (4.1.25),

$$\dot{\mu} = \frac{-1}{E}\left(1 + \frac{E \sin\gamma}{\sqrt{1 - v}}\right) \quad . \tag{4.1.45}$$

Combining these results with equation (4.1.42), obtained by differentiating the QSG condition, leads to

$$\sin\gamma = \frac{-1}{E}\,\frac{(2 - v)\sqrt{1 - v}}{2 + v[\beta(1 - v) - 1]} \tag{4.1.46}$$

and

$$\dot{\mu} = \frac{-1}{E}\left\{1 - \frac{2 - v}{2 + v[\beta(1 - v) - 1]}\right\} \quad . \tag{4.1.45a}$$

These results are plotted in Figure 3. It is seen that the flight path angle is small except for very small velocities. The bank angle rate is close to $-1/E$ except for v close to 0 and 1.

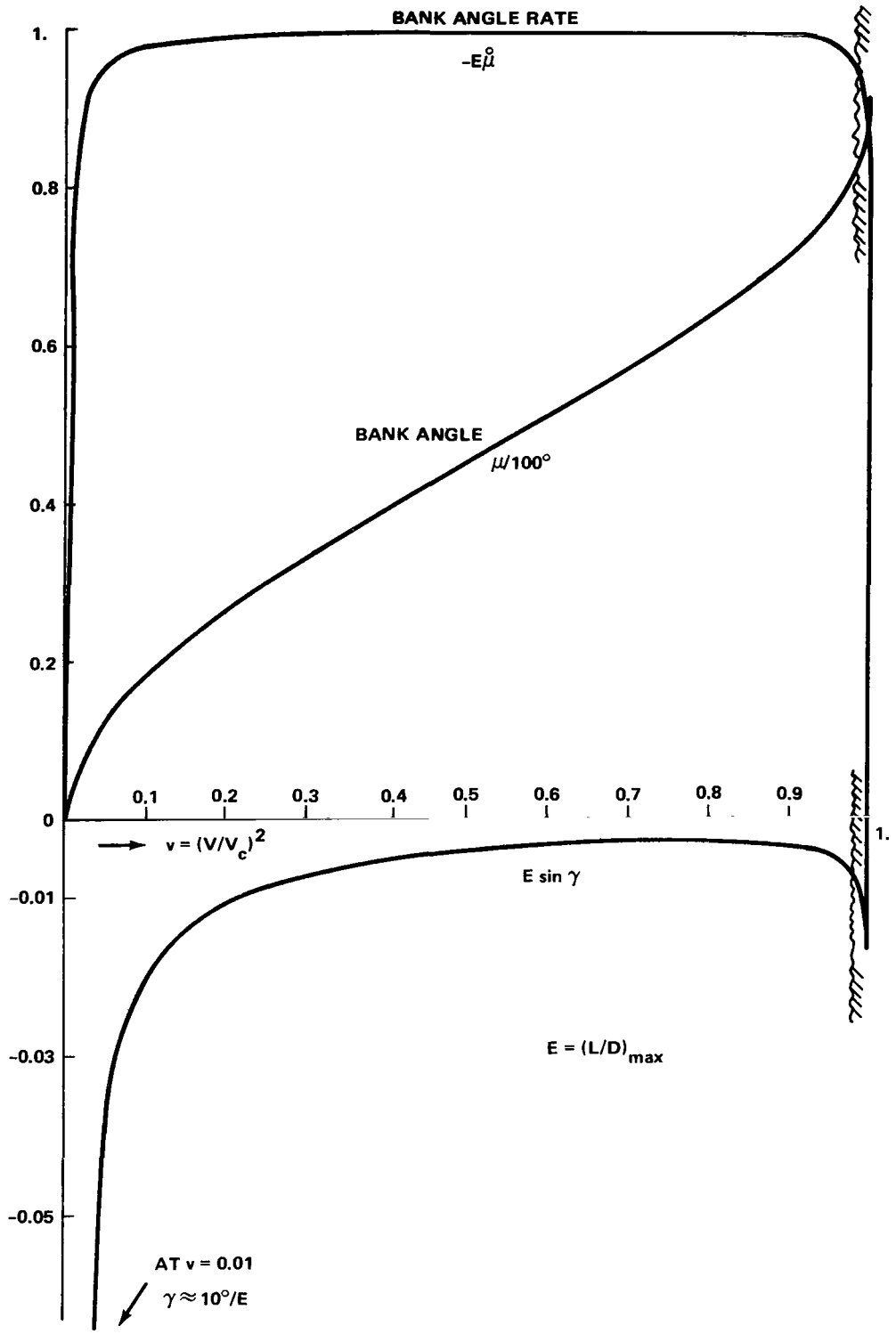

Figure 3. Characteristics of basic QSG maximum range analytical solution.

From the QSG condition, altitude as a function of velocity and lifting factor is

$$h = -\frac{1}{\beta} \ln\left(\frac{\sqrt{1 - v}}{v\, a\, C_{LE}}\right) \quad . \tag{4.1.47}$$

Inserting equations (4.1.25), (4.1.44), and (4.1.46) into equation (4.1.13) yields

$$\overset{\circ}{v} = \frac{-2}{E} \sqrt{v(1 - v)} \left\{1 - \frac{2 - v}{2 + v[\beta(1 - v) - 1]}\right\} \quad . \tag{4.1.48}$$

Neglecting the second term inside the brace [assumption (A11), compare equation (4.1.45a) and Figure 3], this equation may be integrated to yield the final time:

$$t_f = E\left(\tan^{-1}\sqrt{\frac{v_0}{1 - v_0}} - \tan^{-1}\sqrt{\frac{v_f}{1 - v_f}}\right) \quad . \tag{4.1.49}$$

Combining the first two differential equations of equation (4.1.43) yields, with equation (4.1.44),

$$\chi - \chi_0 = E\left(\sqrt{v_0} - \sqrt{v}\right) \quad . \tag{4.1.50}$$

This equation neglects the centrifugal term in the heading differential equation so that for larger cross-ranges the actual heading angle will be smaller. Figure 4 shows how the inertial term grows with increasing lift-to-drag ratio. For $L/D = 3$, the inertial summand averages about 15 percent of the aerodynamic one.

For orbital reentry with $v_0 = 1$ and $v_f = 0.01$, equation (4.1.50) predicts a final heading of $\chi_f > \pi/2$ for vehicles with $E > \pi/1.8 = 1.75$. Some results for other initial and final conditions and the vehicles parameters given in Table 1 are shown in column 8 of Table 2.

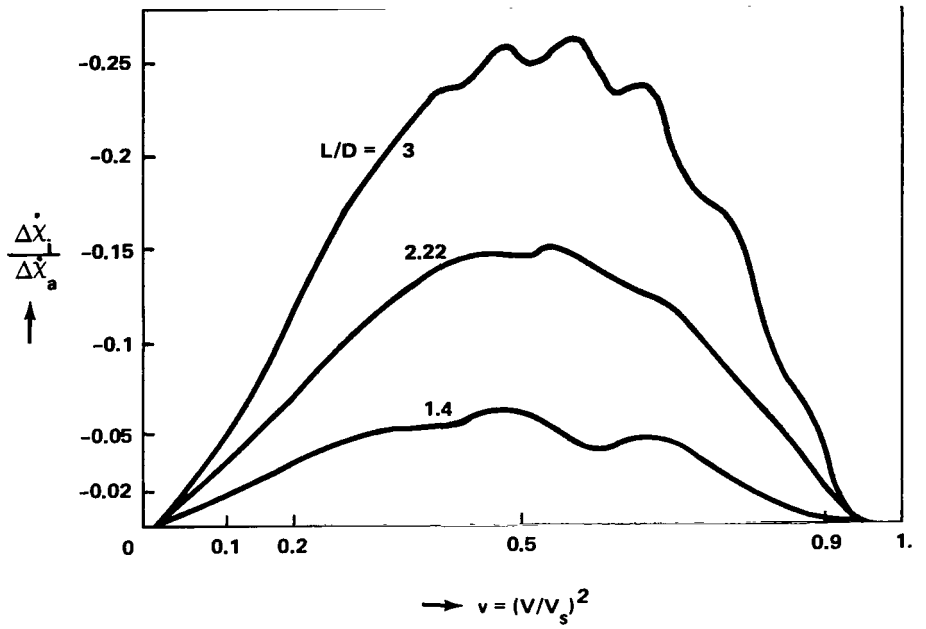

Figure 4. Numerical check on assumption (A11a) for maximum lateral range trajectories.

TABLE 1: VEHICLE CHARACTERISTICS

E = L/D	C_{D0}	k	n	$\frac{C_{LE}S}{m}\Big/\left[\frac{m^2}{kg}\right]$	Wing Loading $m/S/[kg/m^2]$
1.4	0.109	1.45	2.18	0.001885	150
2.22	0.04	1.	1.86	0.000768	250
2.38	0.04	0.95	1.91	0.0008	250
3.	0.028	1.46	2.21	0.000612	250

TABLE 2. MANEUVER TIME AND FINAL HEADING FROM ANALYTICAL SOLUTIONS

1	2	3	4	5	6	7	8
			Maneuver times (t/sec)				
				Cross-range			
L/D	v_0	v_f for $\mu = 0$ at h_f = 30km	Downrange eq. (4.1.54)	eq. (4.1.53)	eq. (4.1.49)	Numerical QSG	χ_f eq. (4.1.50)
1.40	0.90850	0.00822	2024.	1371.	1338.	1340.	69.
1.40	0.95000	0.00822	2382.	1471.	1431.	1458.	71.
1.40	0.98180	0.00822	2968.	1583.	1534.		72.
2.22	0.90850	0.01990	3118.	2112.	2030.		103.
2.22	0.95000	0.01990	3684.	2275.	2178.	2193.	106.
2.22	0.98180	0.01990	4613.	2460.	2341.	2382.	108.
3.00	0.90850	0.02490	4171.	2826.	2702.	2747.	137.
3.00	0.95000	0.02490	4937.	3049.	2902.	2880.	140.
3.00	0.98180	0.02490	6192	3302.	3122.		143.

By assuming a linear bank angle program with time as suggested by equation (4.1.45a) and Figure 3, the QSG differential equation for the velocity may be written as

$$\dot{v} = -\frac{2}{E}\,\frac{\sqrt{v}\,(1 - v)}{\cos\,(\mu_0 - \alpha t)}$$

or

$$\frac{dv}{\sqrt{v}\,(1 - v)} = -\frac{2}{E}\,\frac{d\tau}{\cos\,\mu_0 \cos\,\alpha\tau + \sin\,\mu_0 \sin\,\alpha\tau}\quad , \qquad (4.1.51)$$

which integrates to

$$\ln\left[\frac{1 + \sqrt{v}}{1 - \sqrt{v}}\right]_0^f = \frac{2}{E\alpha}\,\ln\left\{\tan\left[0.5\left(\alpha\tau + \frac{\pi}{2} - \mu_0\right)\right]\right\}_0^f \quad . \qquad (4.1.52)$$

Requiring $\mu_f = 0$ at the final point v_f leads to

$$\tau_{f,L} = \tau_{f,S} \cdot \mu_0 \Big/ \ln\left[\operatorname{ctn}\left(\frac{\pi}{4} - \frac{\mu_0}{2}\right)\right] \quad , \tag{4.1.53}$$

where $\tau_{f,S}$ is Sänger's downrange maneuver time [1]:

$$\tau_{f,S} = 0.5E \ln\left[\frac{(1+\sqrt{v_0})}{(1-\sqrt{v_0})} \; \frac{(1-\sqrt{v})}{(1+\sqrt{v})}\right] \quad . \tag{4.1.54}$$

Columns 4 through 8 of Table 2 show maneuver times for maximum range trajectories ending at $h_f = 30$ km altitude. For conversion to dimensional time, an average value of $\sqrt{r/g} = 815.$ sec has been used. Sänger's downrange result [1] is given in column 4. The next column contains the linear bank-angle-law cross-range maneuver time with μ_0 taken from equation (4.1.44) using equation (4.1.53). The basic solution (4.1.49) yields column 6, which is in surprising agreement with maneuver times obtained from optimizing numerically with the full set of nonlinear differential equations [equations (4.1.1) to (4.1.9) and (4.3.1) through (4.3.9)] and QSG initial condition h_0 and γ_0 determined from equations (4.1.47) and (4.1.46), column 7. Except for the last case shown, the numerical results lie between those of columns 5 and 6. Maximum lateral range trajectories do have a final heading angle in the vicinity of $\frac{\pi}{2}$ relative to the entry direction. From this observation and the numbers shown in column 8 for the final heading angle of the basic solution, the deviation of actual bank angle programs from the basic ones can be guessed. As will be discussed later in connection with the numerical results, optimal QSG maximum lateral range trajectories follow the basic bank angle program initially very closely and deviate from it toward the end, depending on L/D and the velocity range covered.

A full analytical solution to the boundary value problem, equation (4.1.43), has not been found. Two integrals which check favorably with numerical results are the following:

Combining the $\mathring{\lambda}_\chi$ and $\mathring{\lambda}_\Lambda$ differential equations in equation (4.1.43) yields

$$\lambda_\chi \, d\lambda_\chi = -\lambda_\Lambda \, d\lambda_\Lambda$$

with the integral

$$\lambda_\chi^2 + \lambda_\Lambda^2 = 1 \quad , \tag{4.1.55}$$

here the integration constant has been determined from $\lambda_{\Lambda_f} = -1$ and $\lambda_{\chi_f} = 0$. Despite the approximation made, this result agrees very well with numerical solutions to the complete equations (4.1.1) to (4.1.6) as may be seen from Figure 5.

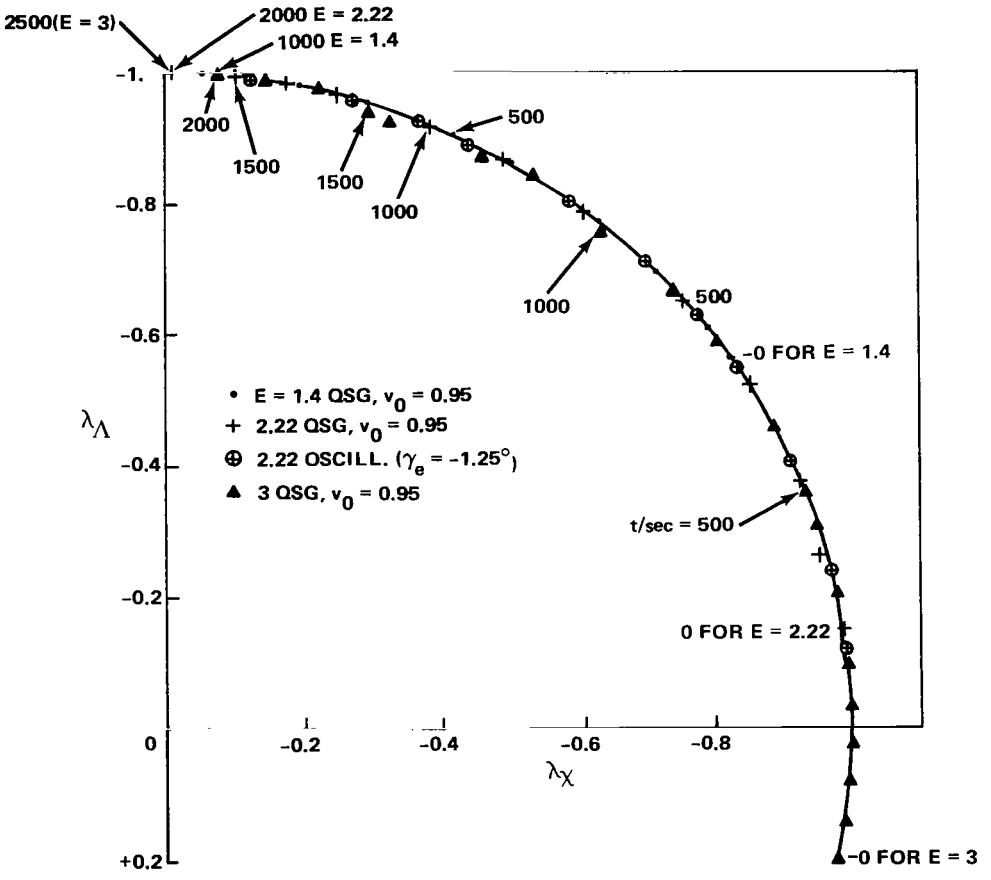

Figure 5. Comparison of analytical approximate result $\lambda_\chi^2 + \lambda_\Lambda^2 = 1$ with numerical solutions.

Combining the $\dot{\Theta}$ and $\dot{\lambda}_\chi$ equation using equation (4.1.53) yields

$$d\Theta = - \frac{d\lambda_\chi}{\sqrt{1 - \lambda_\chi^2}}$$

with the solution

$$\Theta = \Theta_0 + \arcsin \lambda_{\chi_0} - \arcsin \lambda_\chi \quad . \tag{4.1.56}$$

For $\Theta_0 = 0$, the downrange at t_f, then, is

$$\Theta_f = \arcsin \lambda_{\chi_0} \quad . \tag{4.1.56a}$$

4.1.3 NUMERICAL QSG SOLUTIONS

Even though oscillatory trajectories yield maximum range for non-equilibrium initial conditions, QSG trajectories are of special interest since they yield more uniform load distributions and passenger comfort without sacrificing much range. They need not, of course, be flown at maximum L/D if the mission does not require it. In this section, some numerically obtained QSG-footprint trajectories are described.

To get an optimal three-dimensional QSG trajectory, initial conditions have to be matched with the unknown optimal control. This was done in an iteration loop on the initial conditions altitude and flight path angle around the optimization loop to determine the control. The optimization scheme used, a hybrid between the gradient and indirect methods, is especially suited for maximum range footprint computations [24]. The equations of motion underlying these computations are (4.1.1) to (4.1.9) with a drag polar of the form (A8). The adjoint equations are given in section 4.3.

Because of the computational workload involved, trajectories were considered to be reasonably converged QSG when, in the altitude plots, oscillations were hardly recognizable. Some of the trajectories could still be improved with more iterations. A good indication of optimal QSG is that the lift coefficient stays at C_{LE} all the time. It is especially sensitive to non-QSG initial conditions.

Figure 6 shows cross-range versus downrange for maximum cross-range trajectories and three different vehicles (Table 1) from different initial conditions (Table 3).

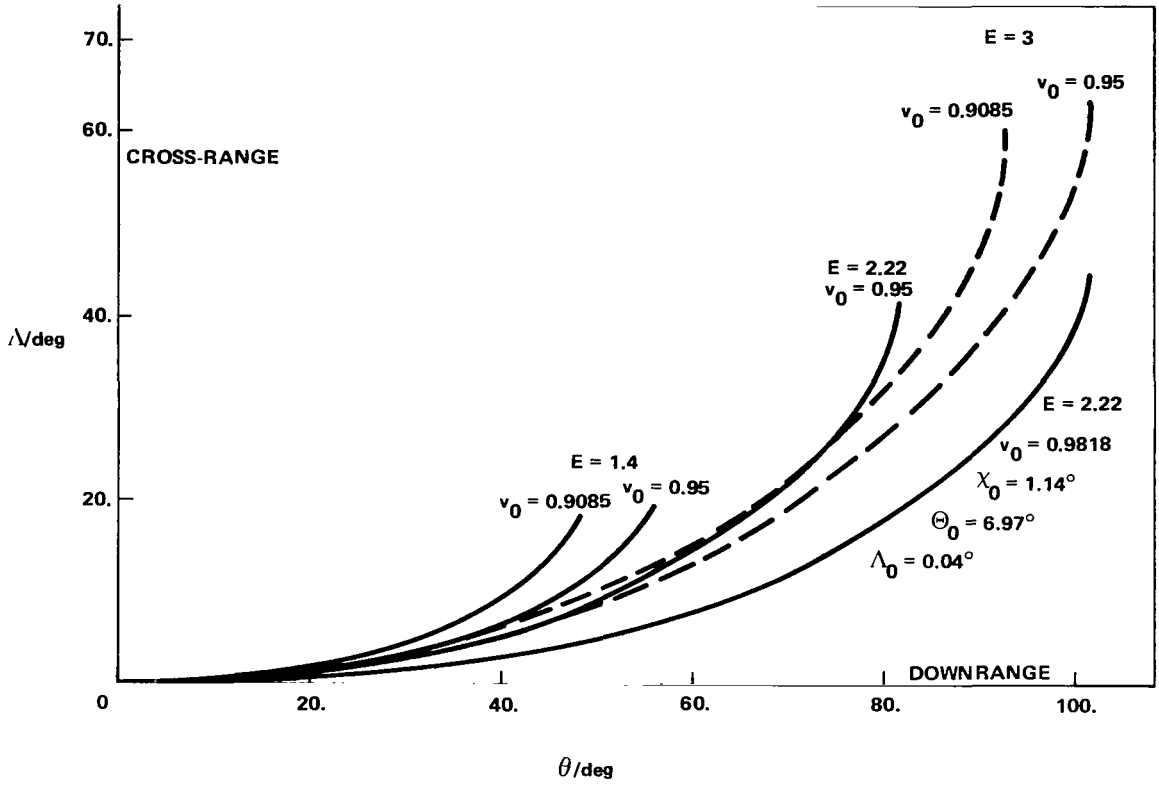

Figure 6. Maximum lateral range QSG trajectories.

TABLE 3. BOUNDARY CONDITIONS FOR MAXIMUM CROSS-RANGE QSG TRAJECTORIES

L/D	v_0	$\gamma_0/0$	h_0/km	$\mu_{0_{QSG}}/0$	Remarks
1.4	0.9085	-0.1729	70.74	72.4	h_f = 30 km
	0.95	-0.2125	73.04	77.1	QSG final conditions
2.22	0.95	-0.134	66.85		see section 4.3.3
	0.9818	-0.182	70.37	82.4	
3.	0.9085	-0.0804	63.59		
	0.95	-0.0994	65.28		

A comparison of the (L/D = 2.22 , v_0 = 0.9818) - QSG trajectory with an oscillatory maximum cross-range trajectory with a flight path angle of γ_0 = -1 deg in h_0 = 64 km altitude is given in Figure 7a. It is seen that the downrange is decreased by about 20 percent and that the cross-range remains the same. The corresponding controls are shown in Figures 7b and c. From Figure 7d, it may be seen that the oscillatory trajectory in an altitude-velocity plot centers around the QSG solution (see also section 4.2 on perturbations). Below V = 2 km/s , both trajectories are very similar.

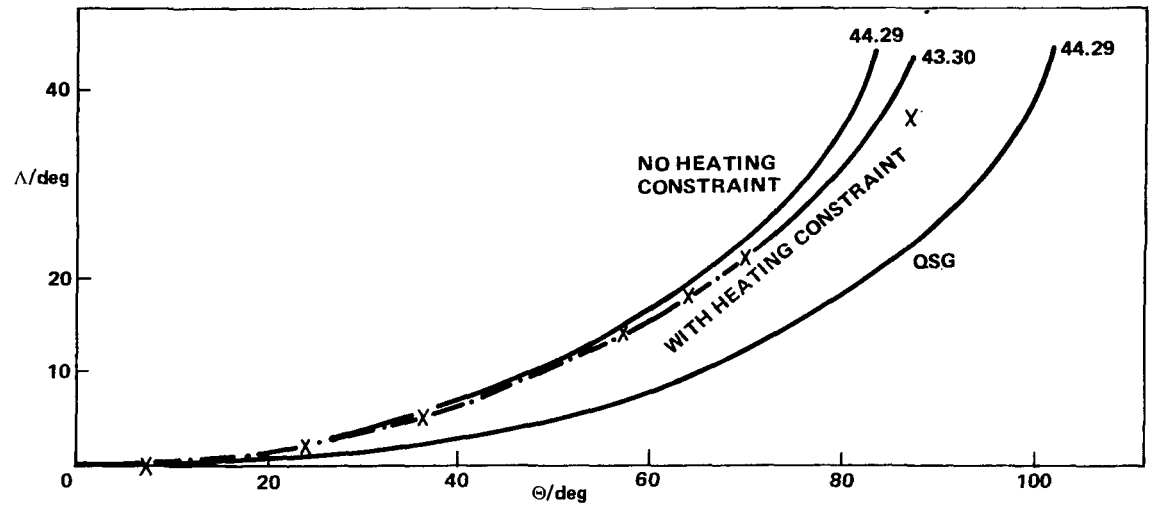

a. Range angles.

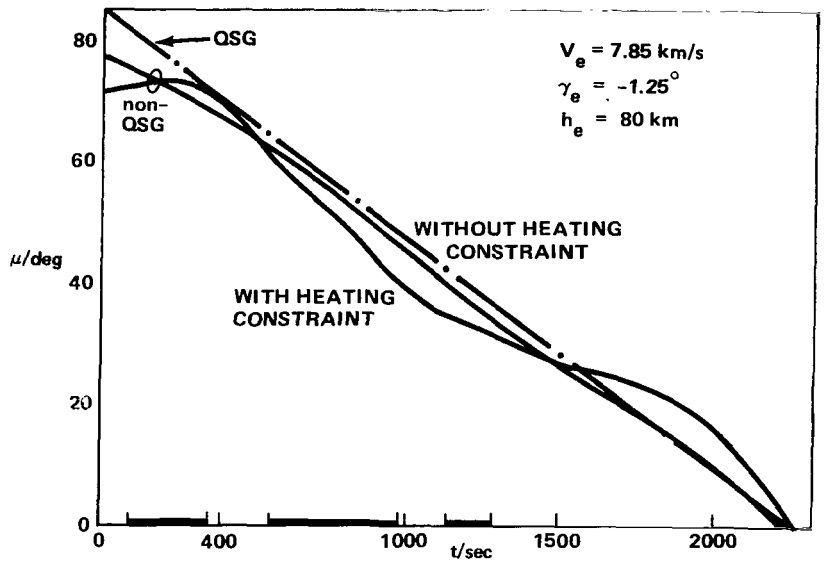

b. Bank angle time histories.

Figure 7. Maximum lateral range orbiter reentry
L/D = 2.22 , m/F = 250 [kg/m^2].

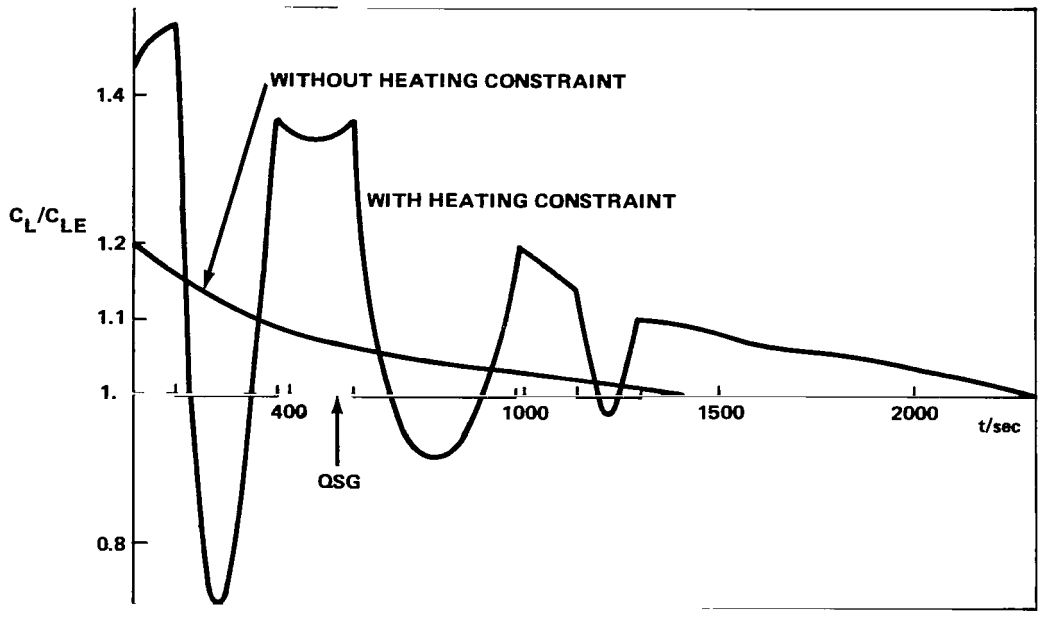

c. Lift coefficient.

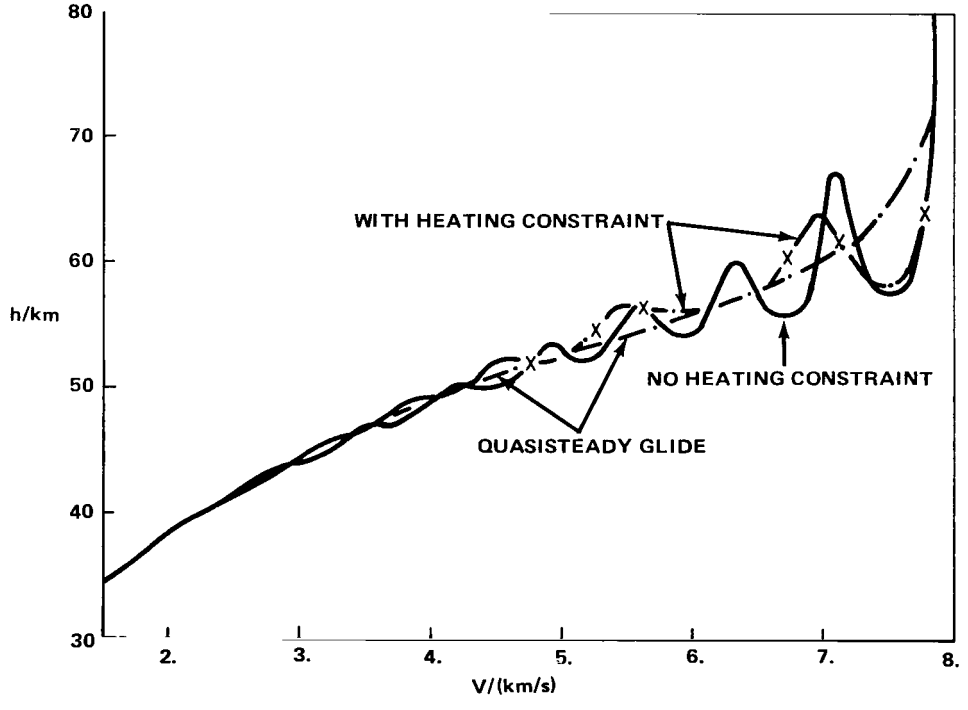

d. Altitude versus velocity.

Figure 7. (Concluded).

The bank angle time histories in Figure 8 for $v_0 = 0.95$ indicate the validity of the basic solution bank angle rate. Initially, it is very closely $1/E$, and it increases or decreases toward the end, depending on the lift-to-drag ratio E. For maximum cross-range, the final heading angle χ_f is in the vicinity of 90 deg relative to entry. The analytical basic solution yields smaller values of χ_f, equation (4.1.50), for $E = 1.4$ and larger ones for $E = 2.22$ or 3. Figure 9 shows how the adjustment in the bank angle program is made by increasing the bank angle μ at lower velocities for $E = 1.4$ and decreasing it for the higher values. If the initial velocity for $E = 1.4$ is lowered to 0.9085 (dashed curve), the bank angle is increased over the entire trajectory.

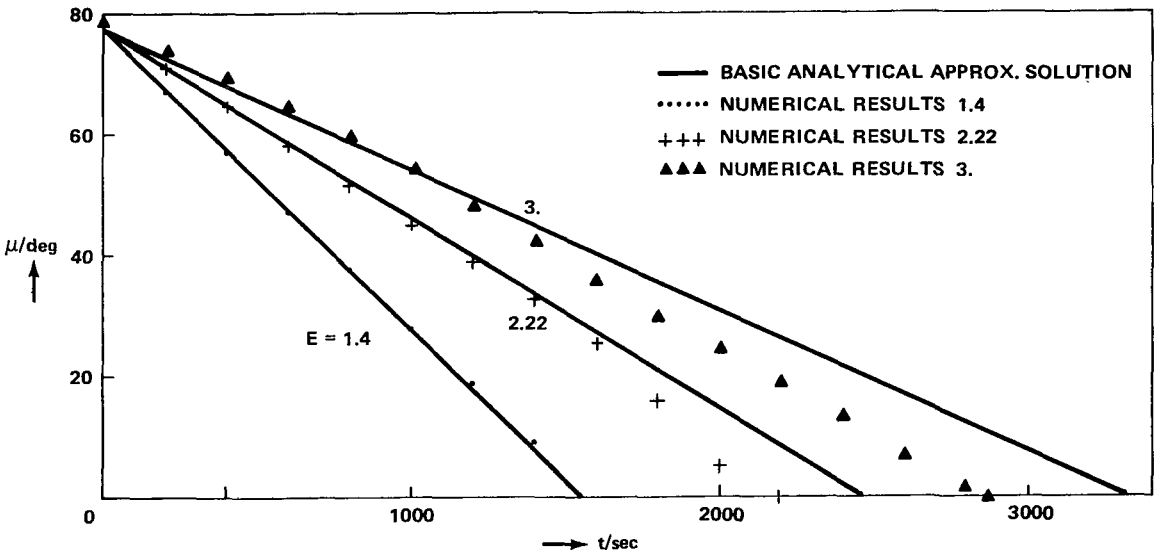

Figure 8. Bank angle time histories for maximum lateral range QSG.

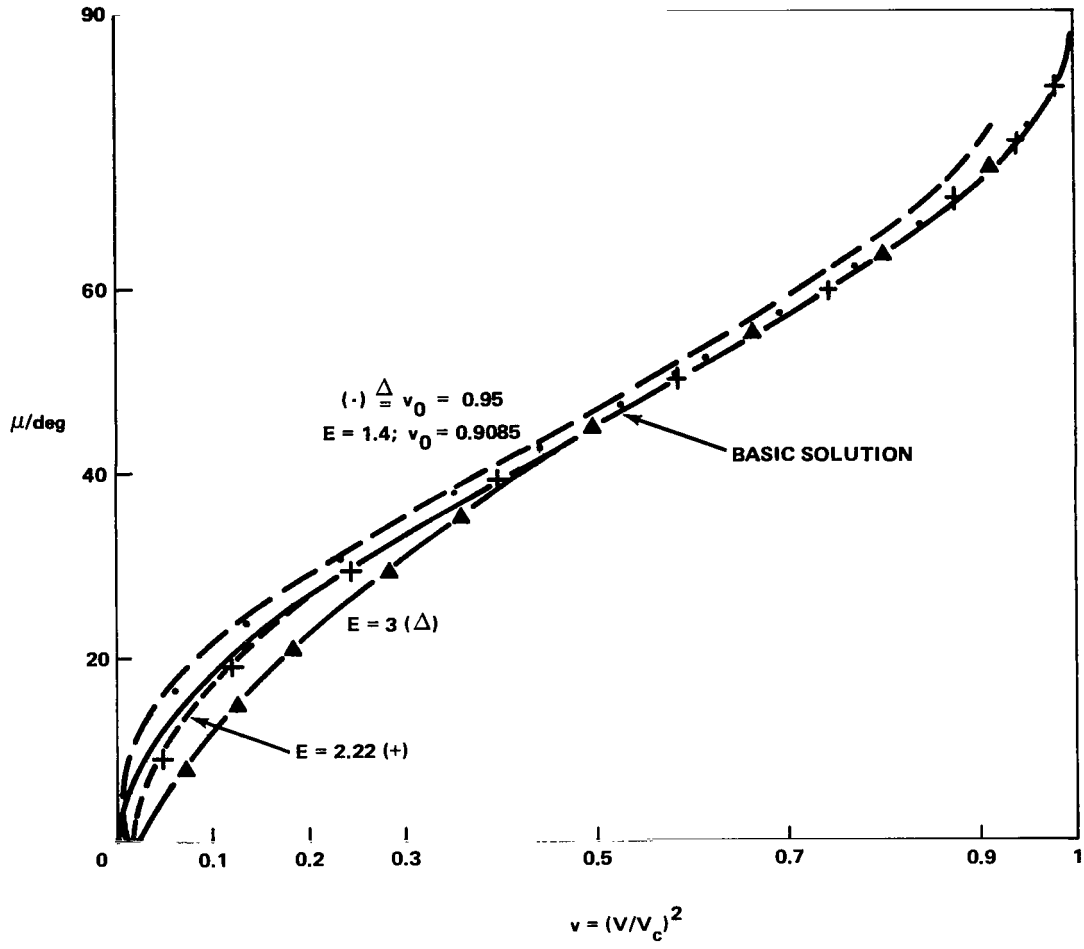

Figure 9. Comparison of bank angle programs between basic analytical approximate QSG solution and numerical solutions for maximum lateral range from same initial conditions.

In Figure 10, QSG trajectories for different points on a footprint are given. It is seen that the bank angle program in the general case is not nearly linear with time. For maximum downrange, μ is of course identically zero.

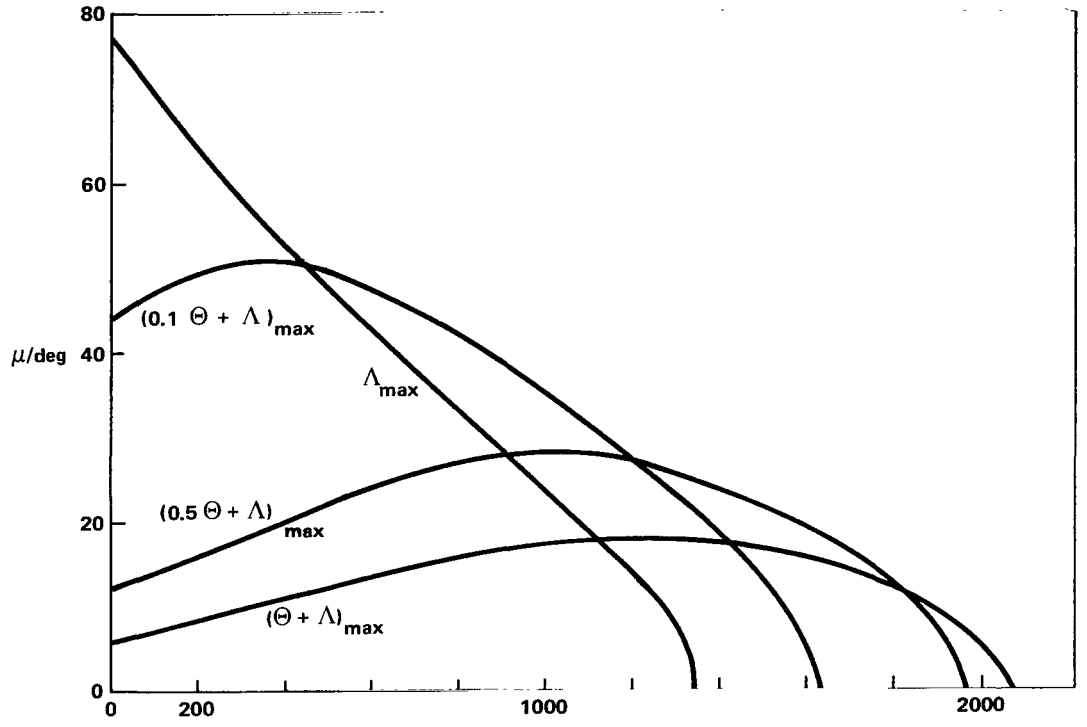

a. Bank angle time histories.

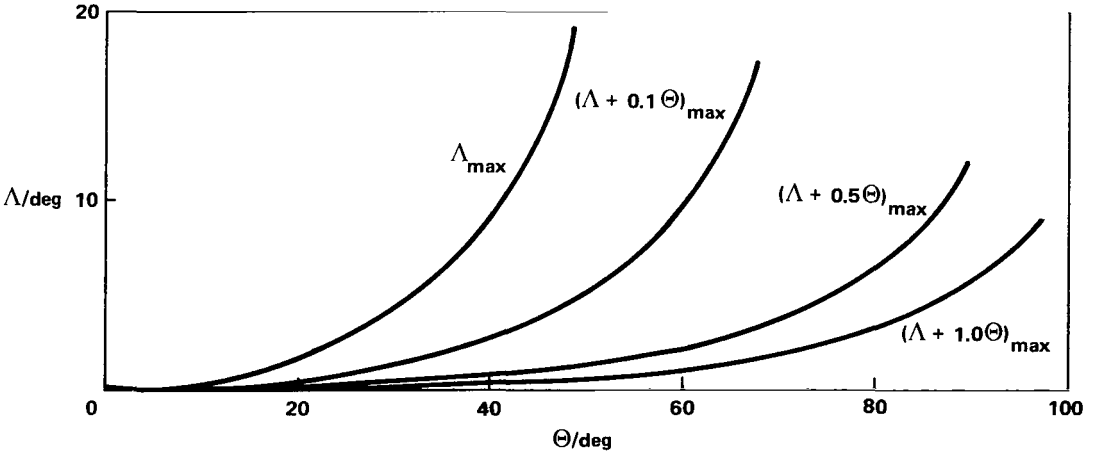

b. Polar ground track (cross-range-downrange).

Figure 10. Maximum range QSG-footprint for $E = 1.4$, $h_f = 30$ km, $V_e = 7.5$ km/sec.

4.2 Perturbation Equations Around Quasisteady Glide

For slightly perturbed initial conditions away from the QSG combination, a good approximation to the actual trajectory may be obtained from series-developing the equations of motion around the QSG state as has been shown for the two-dimensional case in References 4 and 5. In this section, a similar approach is taken for the three-dimensional case based on the basic solution developed in section 4.1.2.

With the state and control variable approximation

$$x = x_Q + \delta x \quad , \qquad u = u_Q + \delta u \tag{4.2.1}$$

where the index Q indicates the QSG solution, a Taylor series expansion of the differential equations (4.1.13) to (4.1.18) yields, with a truncation after the linear term in the perturbation,

$$\left(\overset{\circ}{x}_Q + \overset{\circ}{\delta}_x\right) = f\left(x_Q , u_Q\right) + \left.\frac{\partial f}{\partial x}\right|_Q \delta x + \left.\frac{\partial f}{\partial u}\right|_Q \delta u + \ldots \quad . \tag{4.2.2}$$

Removing the quasisteady glide component leads to the linear set of differential equations with time-varying coefficients

$$\overset{\circ}{x} = Ax + Bu \quad , \tag{4.2.3}$$

where the δ-sign has been dropped for convenience and the coefficient matrices A and B are defined below $\left[\text{for } x^T = (\delta v , \delta\gamma , \delta\chi , \delta\Theta , \delta\Lambda) , \; u^T = \left(\delta C_L , \delta\mu\right)\right]$, with

$$b = \sqrt{v}\; a \exp(-\beta h) \tag{4.2.4}$$

and the QSG condition (4.1.25) introduced into the matrix A ,

$$B^T = \begin{bmatrix} 0 & -2\,bv/E & b\sin\mu & b\cos\mu & 0 & 0 & 0 \\ C_{LE}b\cos\mu & 0 & 0 & 0 & -C_{LE}b\sin\mu & 0 & 0 \end{bmatrix} \qquad (4.2.5)$$

$$A = \begin{bmatrix} -\frac{1}{\sqrt{v}}\left(\frac{3(1-v)}{E\cos\mu}+\gamma\right) & -2\sqrt{v} & \frac{2\beta(1-v)\sqrt{v}}{E\cos\mu} & 0 & 0 & 0 \\ v^{-3/2} & \gamma(1-v)/\sqrt{v} & -\beta(1-v)/\sqrt{v} & 0 & 0 & 0 \\ 0.5v/\sqrt{v} & \sqrt{v} & 0 & 0 & 0 & 0 \\ \chi/(2v) & \sqrt{v}\,\gamma\left(\frac{1-v}{v}\tan\mu+\cos\chi\tan\Lambda\right) & -\beta(1-v)\tan\mu/\sqrt{v} & \sqrt{v}\sin\chi\tan\Lambda & 0 & \frac{-\sqrt{v}\cos\chi}{\cos^2\Lambda} \\ \frac{\cos\chi}{2\sqrt{v}\cos\Lambda} & -\sqrt{v}\,\gamma\frac{\cos\chi}{\cos\Lambda} & 0 & \frac{-\sqrt{v}\sin\chi}{\cos\Lambda} & 0 & \frac{\sqrt{v}\cos\chi\tan\Lambda}{\cos\Lambda} \\ \sin\chi/(2\sqrt{v}) & -\sqrt{v}\,\gamma\sin\chi & 0 & \sqrt{v}\cos\chi & 0 & 0 \end{bmatrix} \qquad (4.2.6)$$

4.2.1 FROZEN STATE APPROXIMATION

Under the assumption that the variables on the reference trajectory are constant, momentary natural frequencies and damping of the perturbation motion can be computed. From the matrix A , equation (4.2.5), it is seen that the vertical motion is uncoupled from the rest (upper left quadrant). It has the characteristic equation (Laplace transform):

$$\frac{s^3}{(1-v)} + s^2\left(\frac{3}{E\cos\mu} - \gamma\right) + s\left[\beta v\left(\frac{\gamma}{E\cos\mu} - 1\right) - \frac{3}{E\cos\mu} - \frac{2}{(1-v)}\right]$$

$$+ \beta v\left\{\gamma + [(1-v)\gamma^2 - (1-3v)]/(E\cos\mu\right\} = 0 \quad ,$$

which over a wide region of v with $\gamma << 1$ and $1 << \beta v$ can be approximated by

$$\frac{s^3}{(1-v)} + s^2\frac{3}{E\cos\mu} - s\beta v + \beta v\left(\gamma - \frac{1-3v}{E\cos\mu}\right) = 0 \quad . \qquad (4.2.7a)$$

In Figure 11 the eigenvalues (period, damping) for the basic solution with $\cos\mu = \sqrt{1-v}$ are plotted against the velocity parameter v using equation (4.2.7).

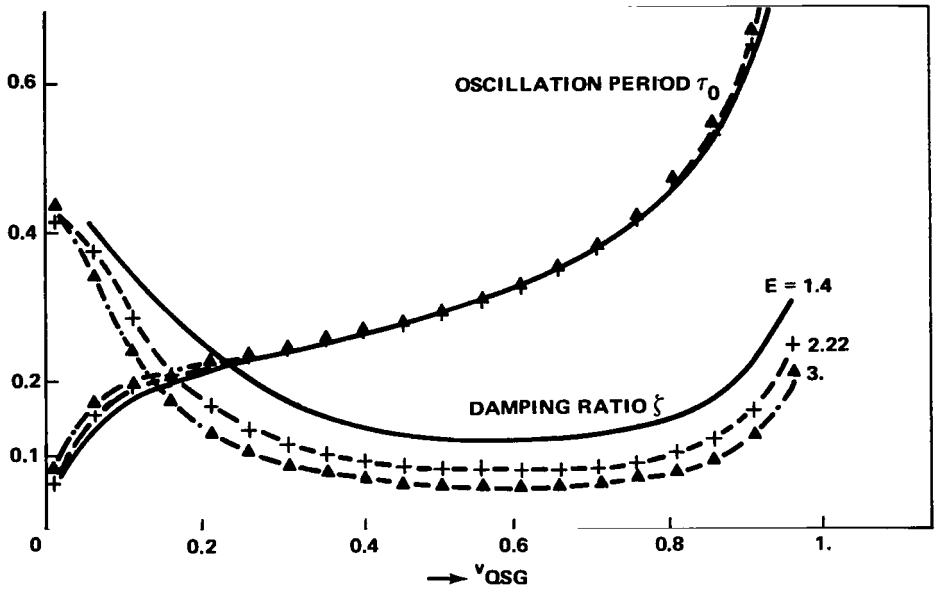

a. Period and damping ratio of oscillatory component.

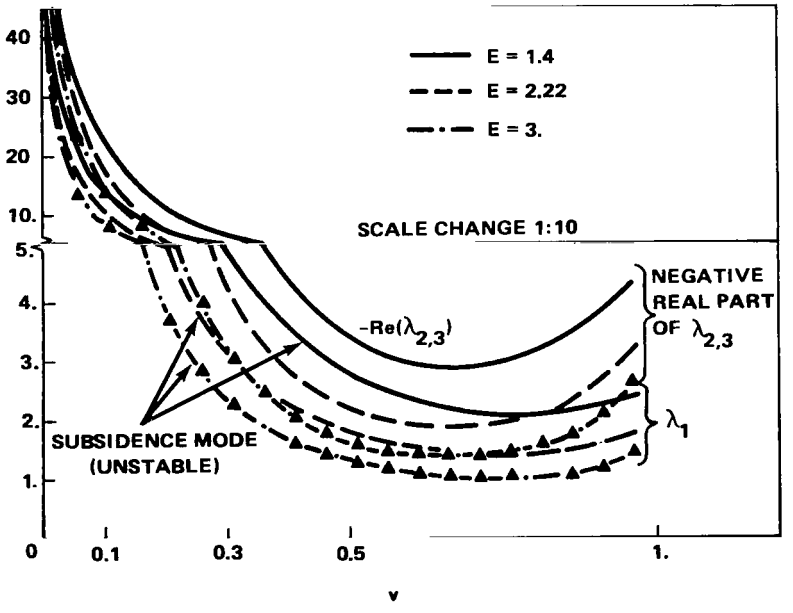

b. Unstable real root λ_1 and oscillatory damping term.

Figure 11. Frozen state perturbation around basic QSG solution.

From Figure 11a, it may be seen that the oscillation period, given in nondimensional time, is almost independent of the lift-to-drag ratio and decreases monotonically with deceleration. The damping ratio decreases with $E = L/D$ increasing; as function of the velocity parameter v, it has a minimum around $v = 0.6$ and assumes values around $\zeta = 0.4$ for small v. Figure 11b shows the unstable real root λ_1 and the damping term of the oscillatory component. Though opposite in sign, they follow the same trend characterized by a sharp increase in absolute value for $v \leq 1/3$. For vehicles with higher L/D the subsidence mode is less unstable.

4.2.2 NUMERICAL INTEGRATION OF PERTURBATION EQUATION

For a linear bank angle law and an initial velocity corresponding to $v_0 = 0.95$, three sets of equations have been integrated to check the approximation of nonlinear oscillatory trajectories by a superposition of a QSG trajectory and linearized perturbation trajectories. The QSG trajectory was computed numerically using the same equations (4.1.13) to (4.1.18), as for the non-QSG trajectory but initial conditions determined from the basic solution. The full set of perturbation equations including the lateral motion but no control perturbation have been used.

Figure 12 shows the altitude perturbation for a vehicle with $E = 1.4$ and $\delta h_0 = \pm 1.46$ km and $\delta\gamma_0 = -\gamma_{QSG} = 0.2125$ deg. The oscillations for unchanged control do not center around $\delta h = 0$ but around a displaced divergent curve when plotted over time (Fig. 12a). The period oscillation is well approximated by a medium value of the frozen state results from the previous section. Toward the end, the strong divergence predicted by the frozen state approximation becomes obvious. When the altitude is plotted over the velocity parameter v, however, all perturbed trajectories converge in the final part toward the QSG trajectory (Fig. 12b). As seen from Figure 7b, the optimized oscillatory lateral range trajectory oscillates around the basic solution. This shows that the control change due to non-QSG initial conditions is determined such that (see Figures 7b and c) the altitude oscillation takes place around the optimal QSG values. The lower curve in Figure 12a (dashed) shows the difference between nonlinear non-QSG and QSG trajectory, and it demonstrates the good degree of approximation of the nonlinear solution achieved by the perturbation equations superimposed on a QSG trajectory. For larger initial perturbations and longer maneuver times, the quality of the approximation deteriorates. Figure 13 shows for $\delta\gamma_0 = -0.2875$ deg and $E = 2.22$ the discrepancy between linearized perturbation and nonlinear solution, which to a large extent stems from the first dip. In the nonlinear model, the first maximum in Δh is 20 percent lower than for the linearized equations, resulting in a time shift. The period of oscillation is slightly

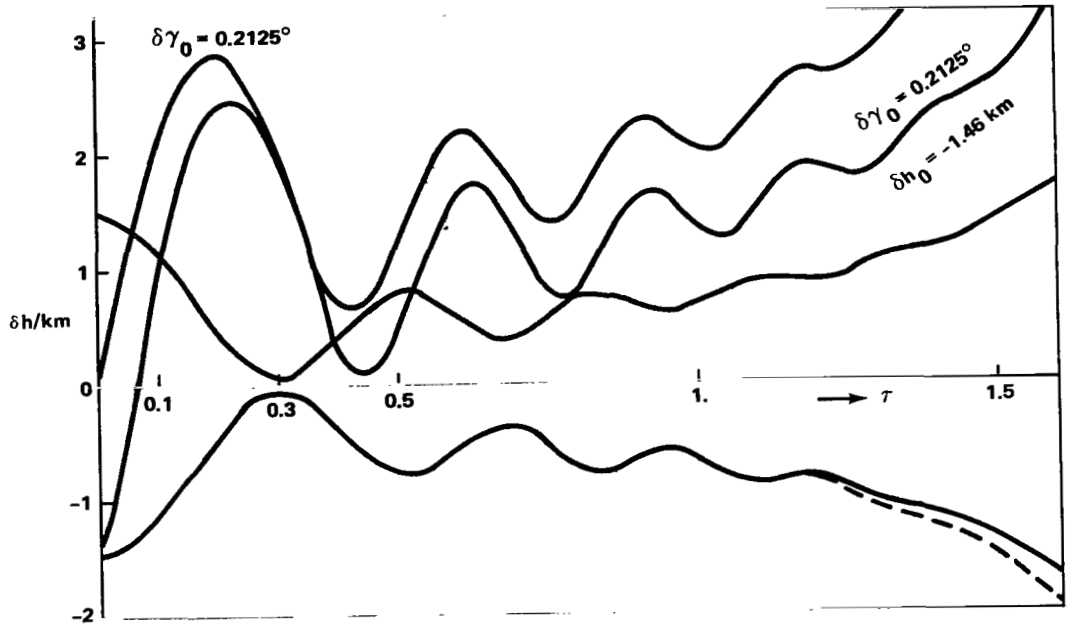

a. Altitude perturbation over time: $\delta h_0 = \pm 1.46$ km and $\delta\gamma_0 = 0.2125$ deg.

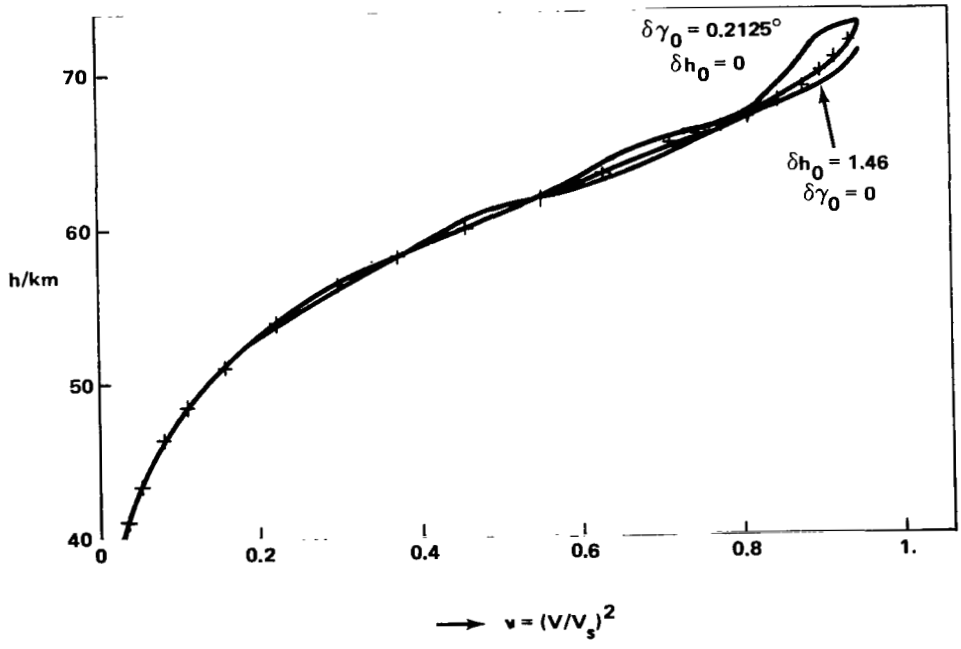

b. Altitude over velocity parameter.

Figure 12. Altitude perturbations for a vehicle with $E = 1.4$, $v_0 = 0.95$.

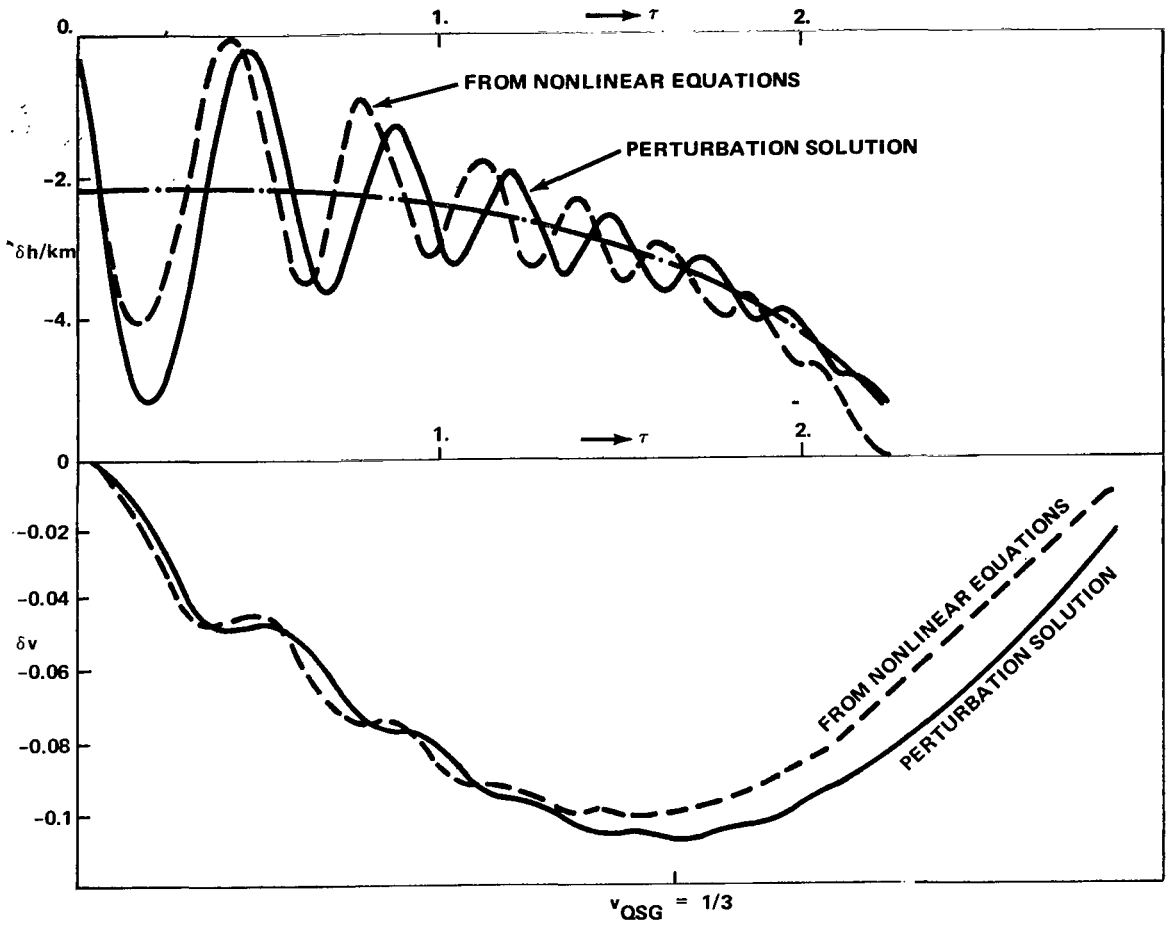

Figure 13. Comparison of perturbation solution to nonlinear results, $E = 2.22$, $v_0 = 0.95$, $\delta\gamma_0 = -0.2875$ deg , $\delta h_0 = 0$.

smaller in the nonlinear case. The general tendency of the nonlinear solution is reflected correctly. The maximum deviation of δv occurs in the vicinity of $v = 1/3$.

The simple linear approximation used here seems to be valid for perturbations of a few tenths of a degree in flight path angle and a few kilometers in altitude only.

4.3 Set of Variational Equations for Numerical Investigations

4.3.1 UNCONSTRAINED ARCS

From equations (4.1) to (4.9) follows, with the Hamiltonian function

$$H = -\lambda_v g \sin\gamma + \frac{V}{r}\cos\gamma\left[\lambda_\gamma(1-gr) - \lambda_\chi \cos\chi \tan\Lambda + \lambda_A \frac{\cos\chi}{\cos\Lambda} + \lambda_\Lambda \sin\chi\right] + \lambda_h V \sin\gamma + \frac{S\rho_0}{2m} V c^{-\beta h}\left[c_A\left(\lambda_\chi \frac{\sin\mu}{\cos\gamma} + \lambda_\Lambda \cos\mu\right) - V\lambda_v c_W\right], \quad (4.3.1)$$

a set of differential equations for the Lagrangian multipliers according to $\dot{\lambda} = -H_x$:

$$\dot{\lambda}_\Theta = 0 \quad , \quad (4.3.2)$$

$$\dot{\lambda}_v = \frac{\cos\gamma}{r}\left[\frac{\cos\chi}{\cos\Lambda}\left(\lambda_\chi \sin\Lambda - \lambda_\Theta\right) - \lambda_\gamma\left(1 + \frac{g_0 R^2}{V^2 r}\right) - \lambda_\Lambda \sin\chi\right] - \lambda_h \sin\gamma + \frac{S\rho_0}{2m} e^{-\beta h} \times \left[2V\lambda_v c_D - c_L\left(\frac{\lambda_\chi}{\cos\gamma}\sin\mu + \lambda_\gamma \cos\mu\right)\right] \quad , \quad (4.3.3)$$

$$\dot{\lambda}_\chi = \frac{V\cos\gamma}{r}\left[\left(\lambda_\Theta - \lambda_\chi \sin\Lambda\right)\frac{\sin\chi}{\cos\Lambda} - \lambda_\Lambda \cos\chi\right] \quad , \quad (4.3.4)$$

$$\dot{\lambda}_\gamma = \cos\gamma\left(\frac{\lambda_v g_0 R^2}{r^2} - \lambda_h V\right) + \frac{V\sin\gamma}{r} \times \left[\frac{\cos\chi}{\cos\Lambda}\left(\lambda_\Theta - \lambda_\chi \sin\Lambda\right) + \lambda_\gamma\left(1 - \frac{g_0 R^2}{V^2 r}\right) + \lambda_\Lambda \sin\chi\right] - \frac{\lambda_\chi \sin\gamma}{\cos^2\gamma}\frac{S\rho_0}{2m} e^{-\beta h} c_L V \sin\mu \quad , \quad (4.3.5)$$

$$\dot{\lambda}_\Lambda = \frac{V \cos\gamma \cos\chi}{r \cos^2\Lambda} \left(\lambda_\chi - \lambda_\Theta \sin\Lambda \right) \quad , \tag{4.3.6}$$

$$\dot{\lambda}_h = \frac{2 g_0 R^2}{r^3} \left(\lambda_v \sin\gamma + \frac{\lambda_\gamma}{V} \cos\gamma \right) + \frac{V \cos\gamma}{r^2}$$

$$\times \left[\frac{\cos\chi}{\cos\Lambda} \left(\lambda_\Theta - \lambda_\chi \sin\Lambda \right) + \lambda_\gamma + \lambda_\Lambda \sin\chi \right] - \beta \frac{S\rho_0}{2m} e^{-\beta h} V$$

$$\times \left[V\lambda_v c_D - c_L \left(\frac{\lambda_\chi}{\cos\gamma} \sin\mu + \lambda_\gamma \cos\mu \right) \right] \quad . \tag{4.3.7}$$

This set is valid for unconstrained arcs with the controls given by

$$\mu_{opt} = \tan^{-1} \left[\lambda_\chi \Big/ \left(\lambda_\gamma \cos\gamma \right) \right] \tag{4.3.8}$$

and

$$C_{L\,opt} = \left(\frac{-w}{V\lambda_v kn} \right)^{1/(n-1)} \tag{4.3.9}$$

where

$$w = \left[\left(\lambda_\chi \Big/ \cos\gamma \right)^2 + \lambda_\gamma^2 \right]^{1/2} \quad .$$

4.3.2 CONSTRAINED ARCS

On a constrained arc of the form

$$C = h - h_e \left(C_L, V \right) = 0 \quad , \tag{4.3.10}$$

Reference 25, the control is chosen by satisfying the constraint

$$C_{LH} = f_e(h, V) \quad , \tag{4.3.11}$$

and there appear additive terms in the adjoint differential equations (second summand)

$$\dot{\lambda} = -\frac{\partial f}{\partial x}\lambda + \left[\frac{\partial f}{\partial u}\left(\frac{\partial C}{\partial u}\right)^{-1}\frac{\partial C}{\partial x}\right]^T \lambda \quad . \tag{4.3.12}$$

Since the only control involved in C is the lift coefficient C_L and the states involved are h and V, one obtains

$$\dot{\lambda}_{V_c} = \dot{\lambda}_{V_{uc}} + K\frac{\partial C_{LH}}{\partial V} \tag{4.3.13}$$

$$\dot{\lambda}_{h_c} = \dot{\lambda}_{h,uc} - K\frac{\partial C_{LH}}{\partial h} \tag{4.3.14}$$

with

$$K = \frac{S\rho V}{2m}\left[\frac{\lambda_\chi}{\cos\gamma}\sin\mu + \lambda_\gamma\cos\mu - V\lambda_v \, kn \, C_{LH}^{(n-1)}\right] .$$

C_{LH} and its partials are determined according to the model described in section 3.4.

4.3.3 BOUNDARY CONDITIONS

The boundary conditions to these and the state differential equations, equations (4.1.1) to (4.1.9), are as follows: The initial state variables are considered to be given. At the final time the altitude is fixed. $h_f = 30$ km was taken as stopping condition for the integration. With all other state variables open to assume the most favorable values for maximum range, the trajectories end with a flare, trading kinetic energy for range in the final part and the lift coefficient goes to its maximum value [24]. This undesirable boundary layer type of behavior was suppressed by prescribing vertical equilibrium at the final time with a lift coefficient corresponding to maximum L/D. For open final heading $\left(\lambda_{\chi_f} = 0\right)$ it is seen from equation (4.3.8) that the bank angle is $\mu_f = 0$. With altitude, lift coefficient, and bank angle given, equation (4.1.3) can be solved for the QSG velocity $V_f \left(\dot{\gamma}_f = 0\right)$ using equation (4.1.42a) to eliminate the flight path angle γ_f.

However, to reduce the number of adjoint sets to be integrated backward in the min-H-gradient procedure [24], V_f and γ_f were not prescribed directly. In a quasisteady glide state, which is desirable for continuation of the trajectory to landing approach, the Lagrangian multiplier to the velocity is easily determinable from the velocity by a physical consideration. The aerodynamic properties of the vehicle translate the kinetic energy altitude

$$h_{ek} = \frac{V^2}{2g} \tag{4.3.15}$$

into range via the factor $E = L/D$. Therefore, for range R measured in a geocentric angle, there follows for the conditions given at final time

$$\lambda_{V_f} = -\frac{\partial R}{\partial V_f} = \frac{-\partial}{\partial V}\left(E\frac{V_f}{2gr}\right) = -E\frac{V_f}{gr} \quad . \tag{4.3.16}$$

With V_f and λ_{V_f} given, the multiplier λ_{γ_f} can now be determined from equation (4.3.9) for the desired final lift coefficient C_{LE}:

$$\lambda_{\gamma_f} = V_f \lambda_{V_f} \, kn \, C_{LE}^{(n-1)} \quad . \tag{4.3.17}$$

For general range maximization, the payoff quantity is

$$\phi = \Lambda + p\Theta \quad . \tag{4.3.18}$$

$p = 0$ leads to maximum lateral range Λ_{max} and $p >> 1$ leads to maximum downrange Θ_{max}. Therefore, one can expect differences between optimal trajectories only for values of p in orders of magnitude around $1 (p = 10^s$ with $|s| <$ say $3)$ [24]. This payoff quantity leads to final values for the Lagrangian multipliers.

$$\lambda_{\Lambda_f} = -1$$

$$\lambda_{\Theta_f} = \lambda_{\Theta} = -p \quad . \tag{4.3.19}$$

For footprint evaluations with QSG final conditions, the boundary value problem has, thus, been reduced to requiring only the backward integration of one set of adjoint equations without resorting to penalty functions.

5. HEATING CONSTRAINED MAXIMUM LATERAL RANGE NON-QSG ENTRY TRAJECTORY

For the heating constraint modeled in section 3.4 with $\Delta C_{LH} = 0.03$, a maximum lateral range trajectory for a Space Shuttle orbiter-type vehicle has been determined (Fig. 7).

The numerical iteration with a refined gradient program was stopped when the increase in lateral range had become very slow. Of the control update computed from the min-H-feature, only about 1 percent could be used without having the iteration diverge. Figure 7d shows altitude versus velocity for three cases: The dash-dotted smooth curve is a QSG trajectory for comparison, around which the (solid) unconstrained trajectory with $V_e = 7.850$ km/s at 80 km altitude and $\gamma_e = -1.25$ deg is seen to oscillate. There are five peaks in the velocity range down to 4 km/s. The heating constrained trajectory has only three peaks in this region and is shifted upward. This is achieved by a higher lift coefficient (Fig. 7c) and a smaller bank angle (Fig. 7b), initially. When the heating constraint is first encountered, the lift coefficient yields in order not to violate the constraint. The iteration process positioned this dip around the lift coefficient for best L/D. During the first dip, the bank angle is slightly increased to use the lift for a heading change and decrease the upward velocity which would lead to too large a flight path angle at the beginning of the second constrained arc where the heating limit is most severe due to the combined effect of high velocity and beginning gravity pull, no more balanced by the centrifugal force. In this region, the bank angle decreases below the value for the unconstrained trajectory and stays there for a while. After the heating region is passed, the bank angle is increased above that for the unconstrained trajectory to make up for the heading change loss in the earlier parts. As Figure 7a shows, this results in a downrange increase of approximately 4 deg, but the lateral range loss is only about 2 percent. The arcs on the heating boundary are approximately $4\frac{1}{2}$, 7, and $2\frac{1}{2}$ minutes long.

6. CONCLUSIONS

Maximum range, three-dimensional atmospheric entry trajectories for lifting vehicles have been approximated by a superposition of a non-oscillatory quasisteady glide component and solutions to linearized perturbation equations. For the QSG motion, variational equations have been derived. They show that the multiplier to the flight path angle is a linear combination of the other multipliers, which may be the cause of numerical difficulties encountered when applying indirect methods to range maximization.

By applying the maximum principle to the QSG problem, a simple bank angle control law has been obtained without taking the boundary conditions into account. This "basic" control, in comparing it to numerical solutions of the full equations, turns out to be closely followed for maximum lateral range trajectories. Adaptation to the special case is achieved by modifications propagating from the final time backward. Because of the simplicity of this basic control, bank angle equal to arc sin of ratio velocity to local satellite velocity and nondimensional bank angle rate approximately equal to inverse of lift-to-drag ratio, some analytical approximate solutions have been obtained. The maximum cross-range maneuver time can be determined fairly accurately. A full analytical solution, however was not achieved. Numerical QSG solutions are given for Space Shuttle orbiter class vehicles with L/D from 1.4 to 3. For general footprint trajectories, the optimal bank angle program is not linear with time. The perturbation equations around QSG show that the frozen state oscillation period is almost independent of vehicle parameters and depends only on velocity while the damping decreases with increasing L/D . There is an unstable motion component over the entire velocity range, increasing rapidly as v becomes less than 1/3. In this region the damping and the frequency of the oscillatory mode also increase strongly, leading to the almost smooth altitude-velocity curves for all perturbed trajectories at these low velocities. The range of validity of the simple linear perturbation equations is limited to a few tenths of a degree in flight path angle and a few kilometers in altitude.

The influence of an angle of attack (lift coefficient), altitude- and velocity-dependent heating constraint on a maximum lateral range earth-orbit entry trajectory for a Space Shuttle orbiter-type vehicle has been investigated numerically. Although the shape of the control time histories and the trajectory have been changed considerably, the loss in lateral range was only about 2 percent compared to the unconstrained one.

George C. Marshall Space Flight Center
National Aeronautics and Space Administration
Marshall Space Flight Center, Alabama 35812, May 1972

REFERENCES

1. Sänger, E.: Raketen-Flugtechnik. R. Oldenburg, 1933.

2. Eggers, A. J., Jr.; Allen, H. J.; and Neice, S. E.: A Comparative Analysis of the Performance of Long Range Hypervelocity Vehicles. NACA TN 4046, Oct. 1957.

3. Loh, W. H. T, ed.: Entry Mechanics and Dynamics. Reentry and Planetary Entry Physics and Technology, Springer-Verlag, Inc., New York, 1968.

4. Campbell, G. S.: Long Period Oscillations During Atmospheric Entry. ARS J., vol. 29, no. 7, Jul. 1959, pp. 525-527.

5. Hanin, A.: A Solution for Atmospheric Entry Trajectories Deviating from Equilibrium Glide. Toronto University, Inst. f. Aerospace Studies, Apr. 1966.

6. Shi, Y. Y.; Pottsepp, L.; and Eckstein, M.C.: A Matched Asymptotic Solution for Skipping Entry into Planetary Atmosphere. AIAA J., vol. 9, no. 4, Apr. 1971.

7. Shi, Y. Y.: Matched Asymptotic Solutions for Optimum Lift Controlled Atmospheric Entry. AIAA J., vol. 9, no. 11, Nov. 1971.

8. Eggers, A. J., Jr.: The Possibility of a Safe Landing. Space Technology, edited by H. S. Seifert, J. Wiley & Sons, Inc., 1959.

9. Slye, R. E.: An Analytical Method for Studying the Lateral Motion of Atmosphere Entry Vehicles. NASA TN D-325, Sept. 1960.

10. Jackson, W. S.: An Improved Method for Determining the Lateral Range of a Gliding Entry Vehicle. J. Aero. Sci, vol. 28, no. 11, Nov. 1961, pp. 910, 911.

11. Jackson, W. S.: Special Solutions to the Equations of Motion for Maneuvering Entry. J. Aero. Sci., vol. 29, no. 2, Feb. 1962, p. 236.

12. London, H. S.: Comment on Lateral Range During Equilibrium Glide. J. Aero. Sci., vol. 29, no. 5, May 1962, pp. 610, 611.

REFERENCES (Continued)

13. Loh, W. H. T.: Dynamics and Thermodynamics of Planetary Entry. Prentice-Hall, Inc., Englewood Cliffs, New Jersey, 1963, p. 160.

14. Shaver, R. D.: On Minor Circle Turns. AIAA J., vol. 1, 1963, p. 213.

15. Arthur, P. D. and Baxter, B. E.: Observations on Minor Circle Turns. AIAA J., vol. 1, no. 10, Oct. 1963.

16. Pozzi, A. and Fadini, B.: A Numerical Analysis of Lateral Range Calculation and Optimization. Proceedings of the XVII International Astronautical Congress, vol. 4, Madrid, Oct. 1966.

17. Nielsen, J. N.; Goodwin, F. K.; and Mersman, W. A.: Three-Dimensional Orbits of Earth Satellites, Including Effects of Earth Oblateness and Atmospheric Rotation. NASA Memo 12-4-58A, 1958.

18. Dickmanns, E. D.: Fehler bei Wiedereinbrittsbahnrechnungen infolge von Näherungsannahmen. III. Lehrgang für Raumfahrttechnik, Aachen, 1964.

19. Brüning, G. and Dickmanns, E. D.: Zur Genauigkeit analytischer Näherungslösungen für Weidereintrittsbahnen in die Erdatmosphäre. ZfW, 14, Heft 1, 1966.

20. Dickmanns, E. D.: Optimale Dreidimensionale Gleitflugbahnen beim Eintritt in Planetenatmosphären. Raumfahrtforschung, Band 14, Heft 3, May-June 1970.

21. Schadt, G. H.: Aerodynamic Heating Problems and their Influence on Earth Orbit Lifting Entry Spacecraft. AIAA Paper No. 68-1126, Oct. 1968.

22. Dash, M. J.: MDAC Orbiter Temperature Boundaries. S&E-AERO-AT-71-22, Marshall Space Flight Center, Alabama, Nov. 30, 1971.

23. Bolza, O.: Die Lagrangesche Multiplikatorenrgel in der Variationsrechnung für den Fall von gemischten Bedingungen und die zugehörigen Grenzgleichungen bei variablen Endpunkten. Mathematische Annalen, 1907, pp. 370-387.

REFERENCES (Concluded)

24. Dickmanns, E. D.: Optimierung von Flugbahnen durch iterative Anwendung des Maximumprinzips. WGLR-Jahrbuch, 1967, pp. 272-301, (Apr. 1968).

25. Bryson, A. E., Jr.: Denhan, W. F.; and Dreyfus, S. E.: Optimal Programming Problems with Inequality Constraints. I: Necessary Conditions for External Solutions. AIAA J., vol. 1, no. 11, 1963, pp. 2544-2550.

NASA-Langley, 1972 —— 30 M199

"The aeronautical and space activities of the United States shall be conducted so as to contribute . . . to the expansion of human knowledge of phenomena in the atmosphere and space. The Administration shall provide for the widest practicable and appropriate dissemination of information concerning its activities and the results thereof."

—NATIONAL AERONAUTICS AND SPACE ACT OF 1958

NASA SCIENTIFIC AND TECHNICAL PUBLICATIONS

TECHNICAL REPORTS: Scientific and technical information considered important, complete, and a lasting contribution to existing knowledge.

TECHNICAL NOTES: Information less broad in scope but nevertheless of importance as a contribution to existing knowledge.

TECHNICAL MEMORANDUMS: Information receiving limited distribution because of preliminary data, security classification, or other reasons.

CONTRACTOR REPORTS: Scientific and technical information generated under a NASA contract or grant and considered an important contribution to existing knowledge.

TECHNICAL TRANSLATIONS: Information published in a foreign language considered to merit NASA distribution in English.

SPECIAL PUBLICATIONS: Information derived from or of value to NASA activities. Publications include conference proceedings, monographs, data compilations, handbooks, sourcebooks, and special bibliographies.

TECHNOLOGY UTILIZATION PUBLICATIONS: Information on technology used by NASA that may be of particular interest in commercial and other non-aerospace applications. Publications include Tech Briefs, Technology Utilization Reports and Technology Surveys.

Details on the availability of these publications may be obtained from:

SCIENTIFIC AND TECHNICAL INFORMATION OFFICE

NATIONAL AERONAUTICS AND SPACE ADMINISTRATION

Washington, D.C. 20546